

Constitutively active glucagon receptor drives high blood glucose in birds

<https://doi.org/10.1038/s41586-025-08811-8>

Received: 11 April 2024

Accepted: 19 February 2025

Published online: 3 March 2025

Open access

 Check for updates

Chang Zhang^{1,8}, Xiangying Xiang^{1,8}, Jian Liu^{2,8}, Yongjie Huang^{2,8}, Jingwen Xue¹, Qian Sun¹, Song Leng¹, Shaobo Liu², Xuefei He¹, Peng Hu³, Xiangjiang Zhan^{4,5}, Qiang Qiu⁶, Shilong Yang⁷, Jürgen Brosius¹ & Cheng Deng^{1✉}

The maintenance of blood glucose, the body's primary source of energy, is indispensable for overall health and metabolic homeostasis. It is regulated predominantly by the glucagon receptor family which is highly conserved in vertebrates^{1–4}. Compared with other vertebrates, avian blood glucose levels are relatively high^{5,6}, and blood glucose regulatory mechanisms in birds have remained unclear. Here we show that high hepatic expression of the avian glucagon receptor (GCGR) in association with constitutively active G_s signalling is dependent on the interaction of different domains. In vivo experiments showed that expression of constitutively active GCGR in hepatic cells led to correspondingly high blood glucose, rapid hepatic lipid utilization and high metabolic rates via downstream signalling pathway activation in fish, reptiles, birds and mammals. Furthermore, we identified a point mutation proximal to the GCGR gene region in chicken that resulted in reduced GCGR mRNA expression and increased body weight. Overexpressing a natural human GCGR variant (*HsGCGR*(H339R)) with modest constitutive activity in mice demonstrated that high expression of this variant increased blood glucose concentration and reduced body weight. In sum, we find that high expression and constitutive activity of GCGR may have contributed to the evolution of flight in the ancestors of birds.

Birds possess many physiological characteristics that are distinct from those of other vertebrates⁶, one of the most prominent being high blood glucose. Blood glucose levels are tightly regulated during metabolic homeostasis⁷ and, in vertebrates, are maintained by a feedback mechanism around a set point that is characteristic for each species^{8,9}. However, this homeostasis is disrupted in birds^{5,8}. Birds have high blood glucose levels, nearly twice those found in mammals, and sevenfold higher than those of amphibians, which have the lowest blood glucose levels of all vertebrates^{5,10–12} (Supplementary Table 1). Although glucose metabolism is highly conserved between birds, mammals and all vertebrates^{6,8,13}, the mechanisms by which birds maintain high blood glucose levels remain unclear.

G-protein-coupled receptors (GPCRs) have essential roles in physiological processes such as neuronal activities, metabolism and reproduction¹⁴. In all vertebrates, glucose homeostasis is regulated mainly by a subfamily of type B GPCR glucagon receptors, including GCGR, glucagon-like peptide 1 receptor (GLP-1R), GLP-2R and gastric inhibitory polypeptide receptor (GIPR), which exhibit high sequence similarity and functional conservation^{1–4}. Tissue expression profiles of the GCGR family have shown differences between mammals and birds^{15–17}. For example, in chickens, GCGR expression is highest in liver, adipose tissue and muscle¹⁷.

In mammals, GCGR expression is highest in liver, followed by kidney^{15,16}. GCGR regulates glucose metabolism primarily in the liver, including glycogenolysis, gluconeogenesis and glycolysis¹⁸. In vertebrates, gluconeogenesis and glycogenolysis are conserved and occur mainly in the liver, producing approximately 85% of endogenous glucose^{7,19–22}. Glycogen phosphorylase can be found in two different states, glycogen phosphorylase a (GP_a) and glycogen phosphorylase b (GP_b)²³. Glucagon (GCG) induces the rapid phosphorylation of inactive GP_b to form active GP_a, triggering glycogenolysis^{24,25}. G_s activation of GCGR, leading to cyclic adenosine monophosphate (cAMP) accumulation, upregulates phosphoenolpyruvate carboxykinase (PEPCK, encoded by *Pck1* and *Pck2*) and glucose-6-phosphatase (*G6pc1* and *G6pc2*) gene transcription, promoting gluconeogenesis^{25,26}. The GCG–G_s axis also upregulates downstream genes involved in lipid metabolism, such as *Ppara*²⁷.

Constitutive activity, whereby cAMP is produced in the absence of ligand, has been documented for many GPCRs, and underlies various potential physiological functions^{28–30}. Constitutive activity can be further activated by cognate ligands, such as in human adenosine A_{2B} receptor, human histamine H₄ receptor, and human H3 receptor (hH3R)^{31–33}. In this study, we find that the avian GCGR exhibits high constitutive activity and maintains high expression levels in the liver.

¹Department of Respiratory and Critical Care Medicine, Center for High Altitude Medicine, Institutes for Systems Genetics, National Clinical Research Center for Geriatrics, West China Hospital, Sichuan University, Chengdu, China. ²Jiangsu Key Laboratory for Biodiversity and Biotechnology, College of Life Sciences, Nanjing Normal University, Nanjing, China. ³Key Laboratory of Exploration and Utilization of Aquatic Genetic Resources (Ministry of Education), Shanghai Ocean University, Shanghai, China. ⁴Key Laboratory of Animal Ecology and Conservation Biology, Institute of Zoology, Chinese Academy of Sciences, Beijing, China. ⁵State Key Laboratory of Animal Biodiversity Conservation and Integrated Pest Management, Institute of Zoology, Chinese Academy of Sciences, Beijing, China. ⁶School of Ecology and Environment, Northwestern Polytechnical University, Xi'an, China. ⁷College of Wildlife and Protected Area, Northeast Forestry University, Harbin, China. ⁸These authors contributed equally: Chang Zhang, Xiangying Xiang, Jian Liu, Yongjie Huang. [✉]e-mail: dengcheng@wchscu.cn

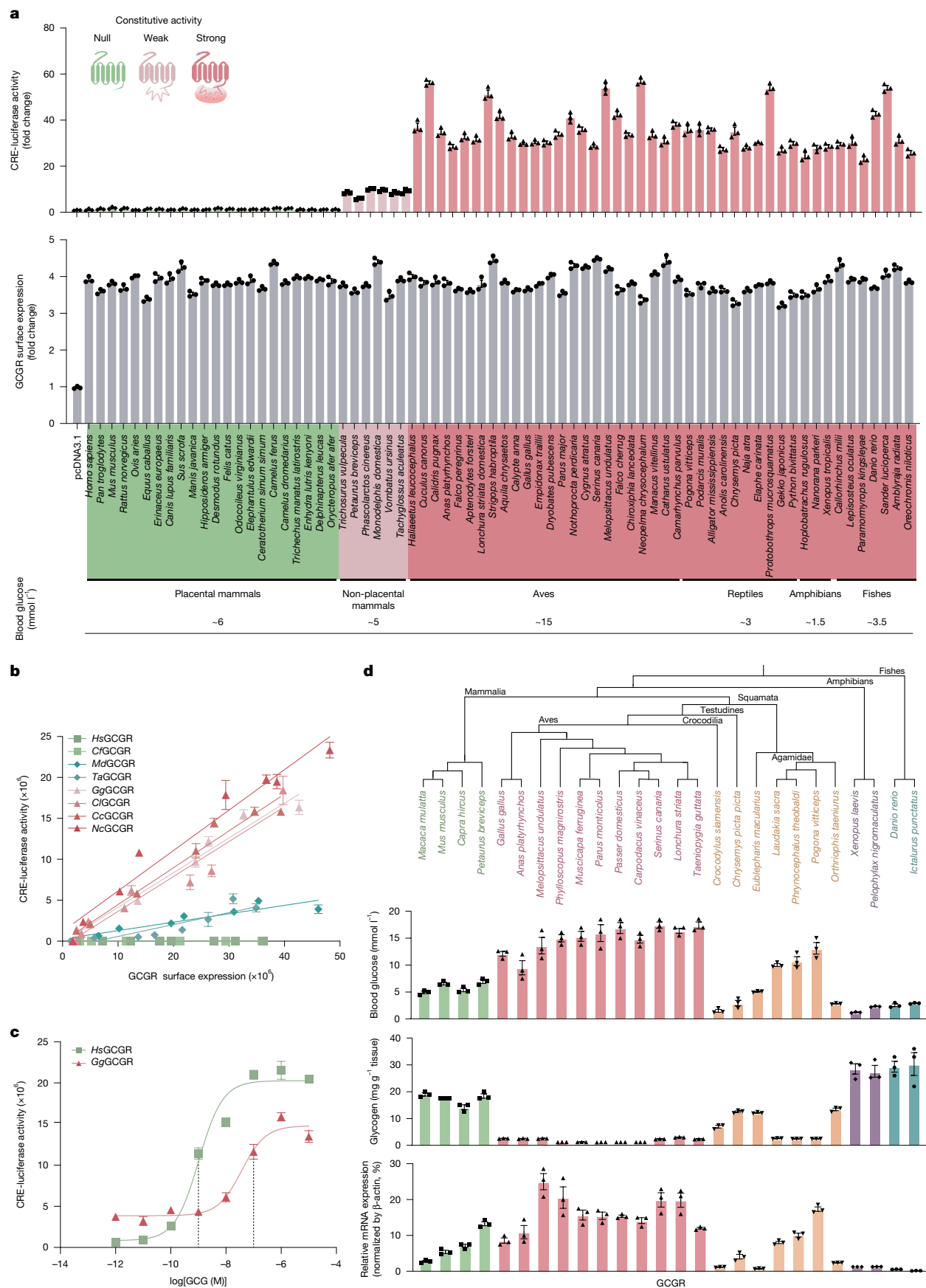


Fig. 1 | See next page for caption.

Fig. 1 | Phylogenetic analysis and functional tests of GCGR in vertebrates.

a, Activation of CRE-luciferase activity (green, no constitutive activity; pink, weak constitutive activity; red, strong constitutive activity) by GCGR homologues from various species (top) at similar protein expression levels (middle). GCGR has constitutive activity in non-placental vertebrates. Bottom, approximate blood glucose concentration. **b**, Constitutive activities of GCGRs (green, placental mammals; blue, non-placental mammals; red, birds). A higher slope indicates a higher level of G_s constitutive activity. *CcGCGR*, *Cuculus canorus*

GCGR; *CfGCGR*, *Camelus ferus* GCGR; *ClGCGR*, *Chiroxiphia lanceolata* GCGR; *MdGCGR*, *Monodelphis domestica* GCGR; *NcGCGR*, *Neopelma chrysocephalum* GCGR; *TaGCGR*, *Tachyglossus aculeatus* GCGR. **c**, Concentration-response curves of GCG stimulation of GCGRs in HEK293. **d**, Blood glucose, glycogen and GCGR mRNA expression (normalized to β -actin gene expression) in the liver of different species. $n = 3$ per group (green, mammals; red, birds; yellow, reptiles; purple, amphibians; blue, fish).

Constitutively active GCGR in non-placental vertebrates

Except for human GIPR, which has weak constitutive activity³⁴, proteins of the glucagon receptor family have been reported to activate signalling pathways solely following stimulation with ligand³⁵. Nonetheless, we investigated the possibility that different members of the glucagon receptor family have constitutive activity using HEK293 cells (Extended Data Fig. 1). Indeed, chicken (*Gallus gallus*) GCGR (*GgGCGR*) produced constitutive cAMP response element (CRE)-luciferase activity that was significantly higher compared with *Homo sapiens* GCGR (*HsGCGR*) (Extended Data Fig. 1a,e). We also found that *GgGCGR*, independent of its ligand GCG, caused significant levels of cAMP accumulation and CRE-luciferase activity compared with *HsGCGR* (Extended Data Fig. 1j–n). *GgGCGR* overexpression significantly increased luciferase activity via G_s signalling, but not through other G-protein signalling pathways (Extended Data Fig. 1o–q). Accordingly, blood glucose levels and GPa enzyme activity in chicken and budgerigar (*Melopsittacus undulatus*) were significantly higher compared with those of mice under fed and fasted conditions (Extended Data Fig. 1s,u). As reported previously^{36,37}, mice showed greater glycogen depletion in response to fasting than birds (Extended Data Fig. 1t). GCGR mRNA expression in liver was upregulated in both mice and birds after fasting (Extended Data Fig. 1v).

To test vertebrate GCGRs for potential constitutive activity, we cloned or synthesized GCGR cDNAs from 22 placental mammals, 6 non-placental mammals, 24 birds, 10 reptiles, 3 amphibians and 7 fishes, and subcloned them into the expression vector pcDNA3.1 (Supplementary Table 2 and Supplementary Fig. 1a). Ex vivo expression of Flag-tagged non-placental vertebrate GCGR constructs resulted in a wide range of protein levels. We detected significantly stronger G_s signalling activity from non-mammalian vertebrate GCGRs, weaker activity from non-placental mammal GCGRs, and no constitutive activity from placental mammal GCGRs, after normalizing by GCGR expression (Fig. 1a). We also assessed whether constitutive activity was correlated with GCGR protein levels. Compared with GCGRs from placental mammals, GCGRs from non-mammalian vertebrates caused high CRE-luciferase activity, whereas GCGRs from non-placental mammals showed weaker activity. Constitutive activity was also found in Urochordata³⁸ GCGRs, indicating that constitutive activity had been lost in placental mammal GCGRs (Supplementary Fig. 1b,c). Furthermore, testing for constitutive activity of GCGRs after domain swapping showed that the constitutive activity of non-placental vertebrate GCGRs was dependent on the cooperation of multiple domains (the stalk, extracellular loop 1 (ECL1), intracellular loop 2 (ICL2) and possibly the C terminus) (Extended Data Fig. 2 and Supplementary Fig. 2). Consistently, previous studies have shown that these domains function in the activation of *HsGCGR* (ICL2 of *HsGCGR* interacts with G_s , as determined from the crystal structure³⁹, and structural differences in the stalk, ECL1 and the C terminus were detected in the activated and inactive *HsGCGR* states^{40,41}) (Supplementary Fig. 3). We next investigated the ability of GCG to further stimulate its corresponding GCGR. GCG stimulated its corresponding receptor with a 50% maximal efficacy (EC_{50}) of 37 nM for *GgGCGR* and 1.04 nM for *HsGCGR* (Fig. 1c). All GCGRs with high constitutive activity could be further activated by human or chicken GCG with similar potency in a dose-dependent manner, but with lower maximal efficacy (E_{max}) than GCGRs with low constitutive activity (Extended Data Fig. 1w–z).

Blood glucose and constitutively active GCGRs

We quantified glycogen content, blood glucose and GCGR expression in the liver of animals with unprotected status and availability, including 11 birds, 4 mammals, 7 reptiles, 2 amphibians and 2 fish species. For a comprehensive list of all animal species and corresponding abbreviations, see Supplementary Tables 3 and 4. Birds and one branch of the reptiles (Agamidae (lizards)) exhibited high constitutive activity and high hepatic expression of GCGR, and had low hepatic concentrations of glycogen stores and relatively high blood glucose levels compared with other vertebrates (Fig. 1d and Extended Data Fig. 3b). Of note, Aves and Agamidae, which had high endogenous GCGR expression, maintained higher blood glucose levels than other vertebrates with similar body weights^{8,42,43}, indicating that high expression levels of constitutively active GCGR may contribute to the differences in blood glucose levels in non-mammalian vertebrates (Fig. 1d, Extended Data Fig. 3c and Supplementary Table 5). Among the non-placental vertebrates, Aves and Agamidae maintained high constitutive activity and hepatic expression of *GCGR* genes throughout their lives (Extended Data Fig. 3e,g). Chicken blood glucose levels increased gradually during incubation and were sustained at high levels throughout life, in parallel with hepatic GCGR expression (Extended Data Fig. 3d,e). In a tuatara reptile (*Pogona vitticeps*), blood glucose and hepatic GCGR expression levels decreased with age, although they remained relatively high (Extended Data Fig. 3f,g).

The basal activity of constitutively active GCGR correlated with GCGR mRNA levels. We observed the highest proportion of hepatic GCGR gene expression in birds, Agamidae and placental mammals (8–20% relative to β -actin gene expression), followed by most reptiles, amphibians and fish (less than 2% relative to β -actin) (Fig. 1d and Extended Data Fig. 3h–j,n–p). Generally, hepatic GCGR protein levels were also high in various species (Extended Data Fig. 3a,i–m,p–u). Endogenous levels of constitutively active *GgGCGR* in the liver of *G. gallus* (about 8% relative to β -actin) exhibited activity that was equivalent to that of non-constitutively active *HsGCGR* stimulated with 100 pM GCG in HEK293 cells (Supplementary Fig. 4a–c). To verify whether GCGR expression levels contributed to physiological effects, we transfected GCGR of different species at their corresponding endogenous hepatic levels into AML12 and HEK293 cell lines, which have negligible endogenous GCGR and GCG gene expression (Supplementary Fig. 4d). We observed that five non-mammalian GCGRs significantly increased the transcription of *Pck1* and *G6pc1*, representing hepatocyte gluconeogenesis, when the relative GCGR expression level reached 8% in AML12 cells (Extended Data Fig. 4a–d). Moreover, the stimulation of *Pck1* and *G6pc1* transcription could be largely inhibited by the protein kinase A inhibitor H89 and the allosteric inhibitor adomeglivant, which inhibits constitutively active GCGR, but not by the G protein $G_{q/11}$ inhibitor YM254890⁴⁴ (Supplementary Fig. 4e–h).

Non-mammalian vertebrate GCGR signalling

To further investigate the role of GCGR in regulating blood glucose and glycogen content, we disrupted hepatic expression of GCGR using the adeno-associated virus (AAV) system in Aves and Agamidae (Fig. 2). Chickens from eggs injected with short hairpin RNA (shRNA)

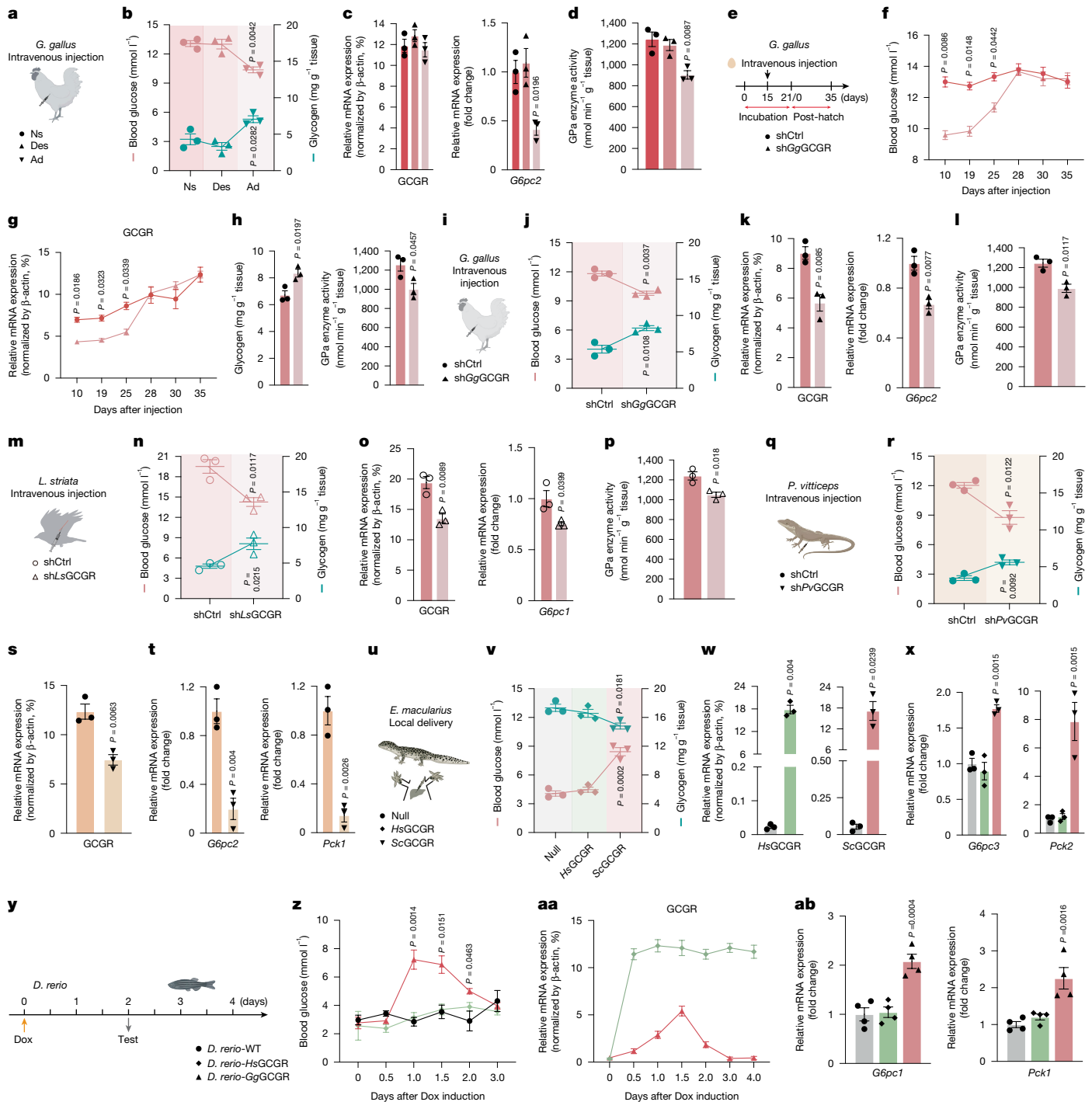


Fig. 2 | Expression of constitutively active GCGRs in liver results in high blood glucose levels in non-mammals. a–d, Intravenous injection in chicks (a). Ns, normal saline; Ad, adomeglivant; Des, des-His¹Pro⁴-glucagon amide. **b–d**, Blood glucose and glycogen content (b), GCGR and G6pc2 expression (c), and GPa enzyme activity (d) four hours after injection. *n* = 3 per group. **e–h**, Intravenous injection of AAV-shGgGCGR in chicken embryo blood vessels (e). **f–h**, Blood glucose (f), GCGR expression (g), and glycogen content and GPa enzyme activity (h) in chicks 19 days after hatching. *n* = 3 per group. **i–l**, Intravenous injection of AAV-shGgGCGR in chicks (i). **j–l**, Blood glucose, glycogen content (j), GCGR and G6pc2 expression (k), GPa enzyme activity (l) ten days after injection. *n* = 3 per group. **m–p**, Intravenous injection of AAV-shLsGCGR in *L. striata* (m). **n–p**, Blood glucose and glycogen content (n), GCGR and G6pc1 expression (o), and GPa enzyme activity (p) four days after injection. *n* = 3 per group. **q–t**, Intravenous injection of AAV-shPvGCGR in *P. vitticeps* (q). **r–t**, Blood glucose and glycogen content (r), GCGR expression (s), and G6pc2 and Pck1

expression (t) five days after injection. *n* = 3 per group. **u–x**, Intrahepatic injection of AAV-HsGCGR and AAV-ScGCGR in *E. macularius* (u). **v–x**, Blood glucose and glycogen content (v), quantification of hepatic HsGCGR and ScGCGR mRNA (w), and G6pc3 and Pck2 expression (x) three days after injection. *n* = 3 per group. **y–ab**, Doxycycline-induced hepatic GgGCGR expression in *D. rerio* (y). **z–ab**, Blood glucose (z), HsGCGR and GgGCGR expression (aa), and Pck1 and G6pc1 expression (ab) 24 h after Dox induction. *n* = 4 per group. Data are mean ± s.e.m. from at least three independent experiments, performed in technical triplicate and were analysed by one-way ANOVA and Dunnett's post hoc test (**b–d**, **v**, **x**, **ab**), two-way ANOVA followed by Šidák's post hoc test (**f**, **g**), two-tailed unpaired Student's *t*-test (**h**, **j–l**, **n–p**, **r–t**), two-tailed unpaired Welch's *t*-test (**w**) or two-way ANOVA followed Tukey's post hoc test (**z**). Cartoons were created in BioRender; Quanwei, Y. (2025) <https://BioRender.com/j11v652>. Sample sizes, statistical methods and *P* values are presented in Supplementary Table 15.

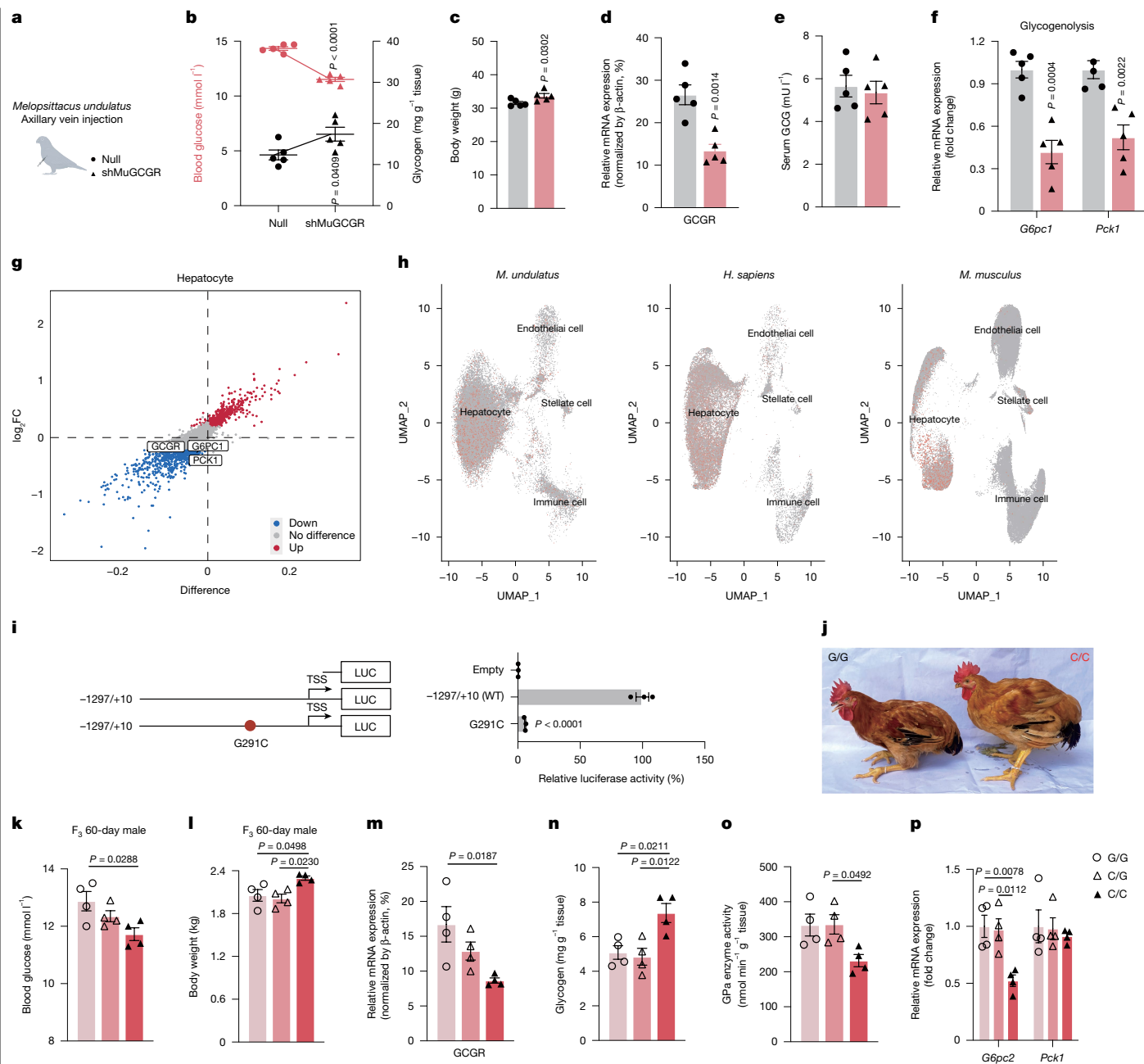


Fig. 3 | Avian constitutively active GCGR regulates high blood glucose by maintaining higher expression levels in liver. **a–h**, Intravenous injection of AAV-shMuGCGR in *M. undulatus* (**a**; created in BioRender; Quanwei, Y. (2025), <https://BioRender.com/j11v652>), $n = 5$ per group. **b–e**, Blood glucose and hepatic glycogen (**b**), body weight (**c**), endogenous hepatic GCGR gene expression (**d**), and serum GCG content (**e**). **f–h**, Hepatic *G6pc1* and *Pck1* expression three days after injection. **g**, Differential gene expression analysis of snRNA-seq data obtained from liver three days after injection ($n = 3$). **h**, Uniform manifold approximation and projection (UMAP) analysis of *M. undulatus* liver snRNA-seq data overlaid with hepatic GCGR gene expression data for *M. musculus*, *M. undulatus* and *H. sapiens* (**h**). **i**, Luciferase (LUC) activity driven by the

chicken promoter mutation G291C. $n = 3$ replicates. WT, wild type. **j**, Images of male F₂ C/C and C/G littermates at the same age. **k, l**, Blood glucose (**k**) and body weight (**l**) of 60-day-old male F₃ C/C, C/G and G/G littermates. $n = 4$ per group. **m**, Hepatic GCGR mRNA expression in 60-day-old male F₃ C/C, C/G and G/G littermates. $n = 4$ per group. **n, o**, Glycogen content (**n**) and GPa enzyme activity (**o**) in liver of 60-day-old male F₃ C/C, C/G and G/G littermates. $n = 4$ per group. **p**, *G6pc2* and *Pck1* expression in 60-day-old male F₃ C/C, C/G and G/G littermates. $n = 4$ per group. Data are mean \pm s.e.m. from at least three independent experiments, performed in technical triplicate. Two-tailed unpaired Student's *t*-test (**b–f**), one-way ANOVA, Dunnett's post hoc test (**i**) and Tukey's post hoc test (**k–p**). TSS, transcription start site.

targeting *GgGCGR* (AAV-sh*GgGCGR*) during incubation exhibited significantly lower blood glucose levels than the control group from day 10 to day 25 after hatching (Fig. 2f), which returned to control levels 1 month post-injection, in parallel with hepatic GCGR expression (Fig. 2f,g). The decrease in receptor expression led to an increase in glycogen content and a decrease of GPa enzyme activity (Fig. 2h). We also injected AAV-sh*GgGCGR* intravenously into 30-day-old chicks

(Fig. 2i), and observed decreased blood glucose levels, GPa enzyme activity and G6PC2 gene transcription, as well as increased hepatic glycogen content compared with controls (Fig. 2j–l). Similar results were obtained in chicks treated with the allosteric inhibitor adomeglivant, which inhibits constitutively active GCGR (Fig. 2a–d and Supplementary Fig. 4i). Reducing hepatic GCGR expression in *Lonchura striata* resulted in a similar pattern (Fig. 2m–p).

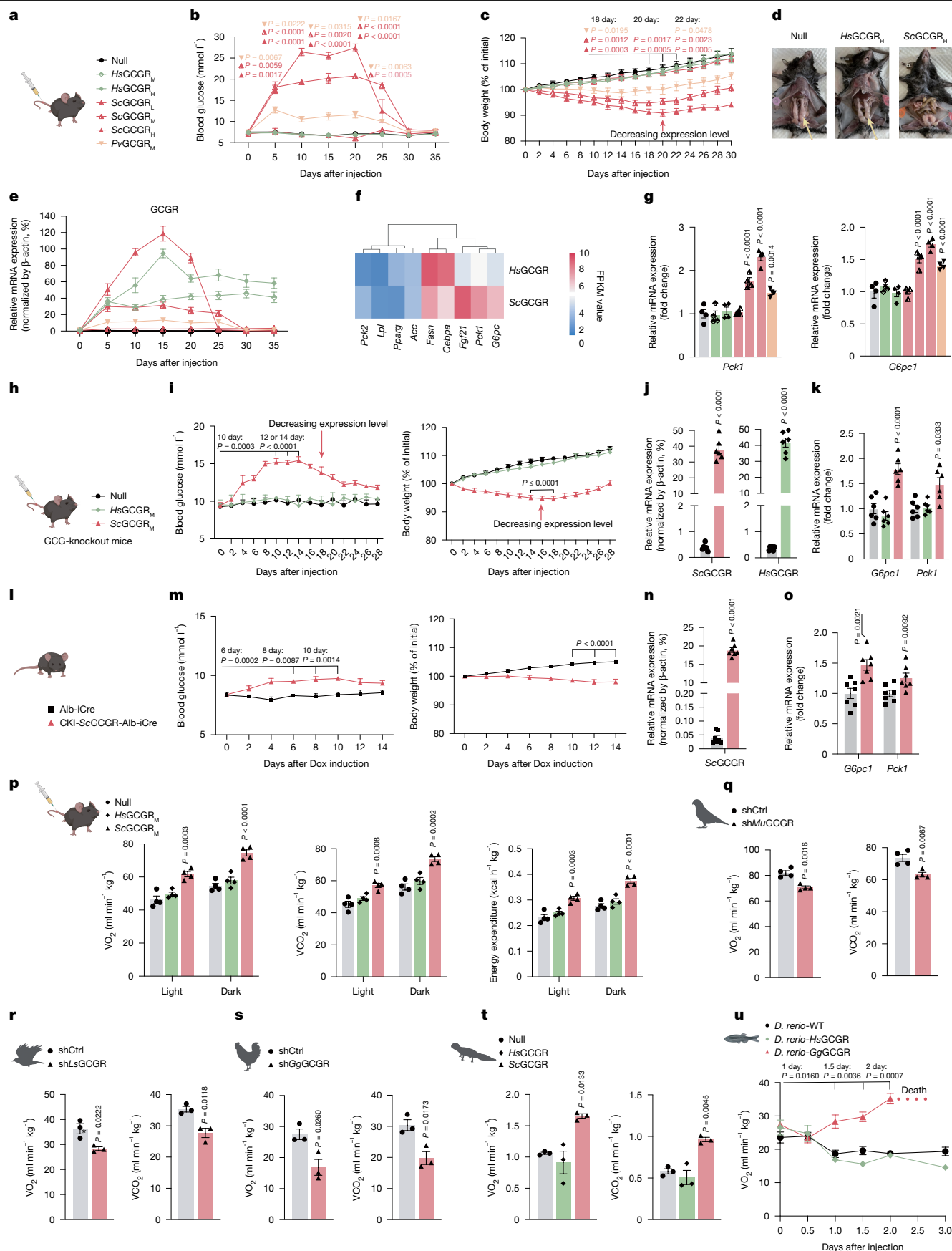


Fig. 4 | See next page for caption.

Fig. 4 | Constitutively active GCGR leads to sustained high blood glucose in mice. **a–g**, Tail vein injections of AAVs in *M. musculus* (**a**; $n = 4$ per group), blood glucose (**b**) and body weight (**c**). Images showing minimal fat accumulation in the ScGCGR_{II} group (**d**), DEGs (**e**), GCGR gene expression (**f**), and *Pck1* and *G6pc1* expression (**g**) 15 days after injection. FPKM, fragments per kilobase of transcript per million mapped reads. **h–k**, AAV tail vein injections in GCG-knockout mice (**h**; $n = 6$ per group), and blood glucose and body weight (**i**). GCGR gene expression (**j**), and *G6pc1* and *Pck1* expression (**k**) 15 days after injection. **l–o**, Dox-induced conditional knockin (CKI) mice (**l**; $n = 7$ per group), and blood glucose and body weight (**m**). ScGCGR mRNA expression (**n**), and *G6pc1* and *Pck1* (**o**) expression 15 days after injection. **p**, VO₂, VCO₂ and energy expenditure of null-, HsGCGR_M- and ScGCGR_M-injected mice fifteen days after injection. $n = 4$ per group. **q**, VO₂ and VCO₂ in budgerigars (*M. undulatus*) four days after injection with control shRNA (shCtrl) or shMuGCGR. $n = 4$ per group. **r**, VO₂ and

VCO₂ in *L. striata* four days after injection with shCtrl or shLsGCGR. $n = 3$ /group. **s**, VO₂ and VCO₂ in *G. Gallus* chicks four days after injection with shCtrl or shGgGCGR. $n = 3$ per group. **t**, VO₂ and VCO₂ in *E. macularius* three days after null, HsGCGR or ScGCGR injection. $n = 3$ per group. **u**, VO₂ in *D. rerio*-HsGCGR and *D. rerio*-GgGCGR over three days. $n = 4$ per group. Data are mean \pm s.e.m. from at least three independent experiments, performed in technical triplicate. Two-way ANOVA followed by Dunnett's post hoc test (**b, c, i, u**), one-way ANOVA and Dunnett's post hoc test (**g, j, k, p, t**), two-tailed unpaired Student's *t*-test (**j, n, o, q–s**), and two-way ANOVA followed by Šidák's post hoc test (**m**). *P* values are shown for the comparison of AAV-ScGCGR_M and null. Cartoons in **a, h, l, p** were created in BioRender; Quanwei, Y. (2025), <https://BioRender.com/i08h417>. Cartoons in **q–u** were created in BioRender; Quanwei, Y. (2025), <https://BioRender.com/j11v652>.

Except for Lacertidae, Varanidae and Iguania, most reptiles had lower blood glucose levels than birds (Extended Data Fig. 4e,g). This might reflect a more important role of hepatic *GCGR* gene expression levels in reptiles or birds (Extended Data Fig. 4f). For example, *P. vitticeps* (Agamidae), which had blood glucose levels close to those of birds (Extended Data Fig. 4e), exhibited decreased blood glucose levels and *G6pc2* and *Pck1* mRNA, as well as increased glycogen content after knockdown of endogenous *GCGR* gene expression (Fig. 2q–t). By contrast, *Eublepharis macularius* (Gekkota), had lower blood glucose levels than Aves and Agamidae. Injection of AAV-null, AAV-HsGCGR (non-constitutively active human GCGR) and AAV-ScGCGR (highly constitutively active *Serinus canaria* GCGR) by local delivery resulted in increased GCGR gene expression (Fig. 2w, Extended Data Fig. 4k,m and Supplementary Video 1). Blood glucose and *G6pc3* and *Pck2* mRNA levels increased, whereas liver glycogen content decreased in the ScGCGR injection group, and no significant changes were detected in the HsGCGR and empty vector (null) groups (Fig. 2u–x and Extended Data Fig. 4l).

To test whether increases of modestly expressed and constitutively active GCGR would increase blood glucose levels, we engineered two transgenic zebrafish (*Danio rerio*-HsGCGR and *D. rerio*-GgGCGR) to enable doxycycline-inducible liver-specific GCGR expression (Fig. 2y and Extended Data Fig. 4n–p). Zebrafish were collected at different time points (0, 0.5, 1, 1.5, 2 and 3 days) after doxycycline induction (Fig. 2y); there was widespread death at day 4. As shown in Fig. 2aa,ab, hepatic GCGR gene expression was increased, and zebrafish with high GgGCGR expression showed sustained increase in blood glucose (6–8 mM) and *G6pc1* and *Pck1* mRNA levels. The GCG–G_s axis also upregulates genes involved in lipid metabolism—we therefore investigated lipid metabolism-related genes of these species (Extended Data Fig. 5). Knockdown of constitutively active GCGR in bird and *P. vitticeps* livers downregulated genes in the lipid metabolism pathway (Extended Data Fig. 5a–i), whereas overexpression of constitutively active GCGR in the liver of *E. macularius* and *D. rerio* upregulated these genes (Extended Data Fig. 5j–n).

snRNA-seq, GCGR and avian glucose metabolism

To investigate the regulatory mechanisms responsible for the high blood glucose levels in birds, we used RNA-mediated interference via intravenous injection of AAV-shMuGCGR to reduce endogenous *GCGR* gene expression in liver of adult male *M. undulatus*. Following injection, transcript levels of the endogenous GCGR gene and blood glucose levels decreased within three days, with a simultaneous increase in body weight and hepatic glycogen (Fig. 3a–d). However, no significant changes were detected in serum GCG levels (Fig. 3e) and the expression of glycogenesis-related genes (*G6pc1* and *Pck1*) decreased after endogenous GCGR knockdown (Fig. 3f). Using single-nucleus RNA sequencing (snRNA-seq), we identified distinct cell clusters that expressed *M. undulatus* GCGR (MuGCGR) in the liver, including Kupffer cells, endothelial

cells, dendritic cells, stellate cells and cholangiocytes (Extended Data Fig. 6a), whereby hepatocytes exhibited the highest GCGR transcription (Extended Data Fig. 6b). We used gene enrichment analysis to identify differentially expressed genes (DEGs) downstream of GCGR (Extended Data Fig. 6c). Decreasing hepatic expression via shMuGCGR led to downregulation of genes related to fatty acid and carbon metabolism (comprising carbohydrate, energy and amino acid metabolism) as well as peroxisome proliferator-activated receptor (PPAR, a group of transcription factors) pathway signalling (Extended Data Fig. 6c). Furthermore, expression of genes related to glycogenesis (*G6pc1* and *Pck1*), lipolysis (*Atgl*), lipogenesis (*Acc*, *Fasn* and *Pparg*) and fatty acid oxidation (*Cpt1a*) was significantly decreased in the AAV-shMuGCGR group (Fig. 3g and Extended Data Fig. 6g–i), consistent with data from quantitative PCR with reverse transcription (RT–qPCR) (Fig. 3f and Extended Data Fig. 6h–j).

For *GCGR* expression analysis at the single-cell level in liver nuclei across species, we compared *M. undulatus* data with public data from *D. rerio*⁴⁵, *Xenopus laevis*⁴⁶, *Mus musculus*⁴⁷ and *H. sapiens*⁴⁸. Our findings indicated that *GCGR* expression was higher in hepatocytes of *M. undulatus*, *H. sapiens* and *M. musculus* compared with *D. rerio* and *X. laevis* (Fig. 3h and Extended Data Fig. 6k,l).

eSNP in the chicken GCGR promoter

Expression single nucleotide polymorphisms (eSNPs) are single nucleotide polymorphisms (SNPs) that are associated with gene expression changes⁴⁹. We used chickens to identify eSNPs associated with blood glucose levels. We grouped Chinese yellow-feathered broilers (outbred) into groups according to high or low blood glucose (Supplementary Fig. 5a) and separately bred an F₁ based on these traits. We sequenced genomic DNA from F₀ and F₁ chickens, revealing a G291C mutation in the *GCGR* gene promoter region that was associated with reduced GCGR expression in liver. At day 60, G291C/G291G (C/G) variants showed lower blood glucose than G291G/G291G (G/G) littermates (Supplementary Fig. 5l). Body weight differences between C/G and G/G individuals emerged at day 90 (Supplementary Fig. 5m), and blood glucose differences disappeared by day 90 (Supplementary Fig. 5m).

G291C/G291G (C/G) homozygous individuals were obtained in F₂. Male C/C individuals had the lowest blood glucose and highest body weight at 60 days (Supplementary Fig. 5q). From days 40 to 60, C/C individuals exhibited the greatest weight gain (Supplementary Fig. 5s). In F₃, C/C individuals exhibited lower blood glucose, reduced GCGR expression and higher body weight than C/G and G/G littermates (Fig. 3k–m). Additionally, the C/C individuals exhibited lower GPa enzyme activity, higher hepatic glycogen content and decreased *G6pc2* expression (Fig. 3n–p). Lipolysis (*Atgl* and *Lpl*) and lipogenesis (*Acc*, *Fasn* and *Cebpa*) genes were also downregulated in C/C individuals (Extended Data Fig. 7b,c), with no changes in serum triglycerides or non-esterified fatty acids (NEFAs) (Extended Data Fig. 7d,e). C/C males exhibited reduced *GCGR* expression in subcutaneous adipose tissue

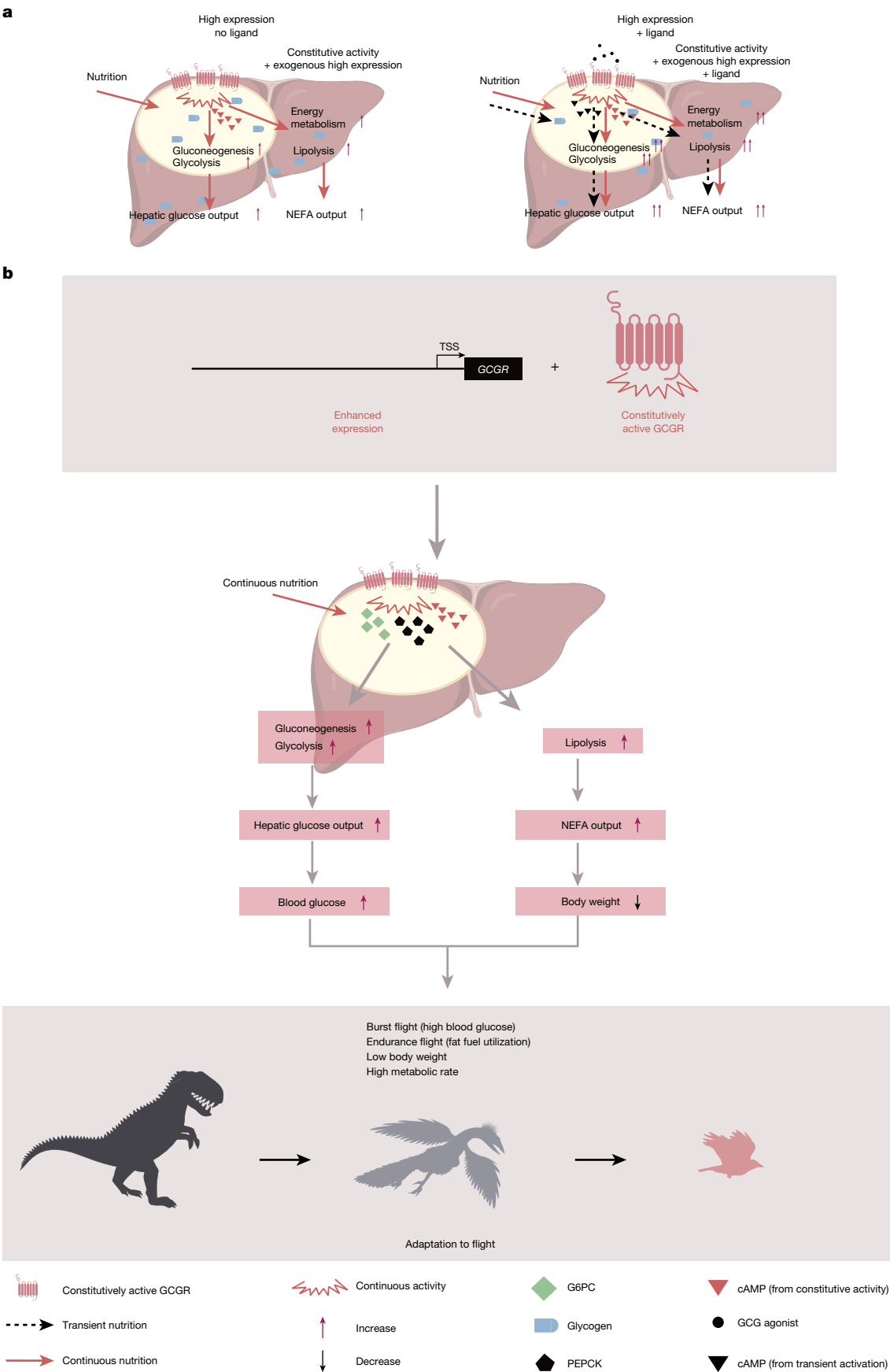


Fig. 5 | See next page for caption.

Fig. 5 | Model of mechanisms regulating the glycaemic effects of constitutively active GCGR. **a**, Model comparing classical ligand-induced activation of GCGRs (right) and constitutive GCGR activity controlling hepatic glucose output. In birds and Agamidae, constitutively active GCGR is highly expressed in liver, activating the G_s signalling pathway and enhancing glucose and lipid metabolism even in the absence of ligand stimulation. Red arrows

show constitutive activity and dashed arrows show ligand-regulated (transient) activity. **b**, Proposed model for the putative role of GCGR in flight adaptation in birds. High expression of constitutively active GCGR in liver upregulates downstream glucose and lipid metabolism and energy metabolism. This is one of the potential factors that facilitated flight in birds. Cartoons created in BioRender; Quanwei, Y. (2025), <https://BioRender.com/c76s860>.

(Extended Data Fig. 7f). Lipolysis (*Atgl* and *Lpl*), lipogenesis (*Acc* and *Fasn*), thermogenesis (*Pparg* and *Pgc1a*) and fatty acid oxidation (*Cpt1a*) genes were also downregulated in the subcutaneous adipose tissue (Extended Data Fig. 7g–j).

Avian-like glucose and weight phenotype in mice

We next introduced different GCGRs including *HsGCGR*, *GgGCGR*, *ScGCGR* and *Protothirops mucrosquamatus* (snake) GCGR (*PmGCGR*) into C57BL/6 mouse livers by adenovirus (ADV) infection, and investigated relevant markers (Extended Data Fig. 8a). We monitored GCGR expression for approximately one week after ADV injection. During this time, blood glucose levels and GPa and PEPCK enzyme activities were significantly increased, whereas glycogen content decreased, with a maximum on day five (Extended Data Fig. 8c–e). Furthermore, *GgGCGR* overexpression resulted in glucose intolerance and insulin resistance on day four (Extended Data Fig. 8g). *Pck1* and *G6pc1* expression and serum insulin levels were significantly increased, whereas serum GCG levels remained unchanged (Extended Data Fig. 8h,i). Expression of GCGRs was maintained only for a short time after ADV injection (Extended Data Fig. 8b). Therefore, AAV was chosen to achieve extended GCGR expression and cDNAs encoding *HsGCGR*, *ScGCGR* and *P. vitticeps* GCGR (*PvGCGR*) were synthesized for AAV vector construction (Fig. 4a). Mice injected with low, medium and high dosages of AAV-*ScGCGR* (*ScGCGR_L*, *ScGCGR_M* and *ScGCGR_H* groups, respectively) showed corresponding low, medium and high blood glucose. The *ScGCGR_M* group exhibited hepatic GCGR expression and concomitant blood glucose similar to the physiological *S. canaria* levels (Figs. 1d, 4b,e), but no increase in glucose levels were observed in the *HsGCGR* and null groups (Fig. 4b), in parallel with insulin levels (Extended Data Fig. 8l). In accordance with *GCGR* gene expression patterns, the alterations in glycogen content lasted nearly one month (Extended Data Fig. 8m), which was similar to the phenotypes of *db/db* mice, except for the lower serum GCG levels in AAV-injected mice (Extended Data Fig. 8n). Glucose tolerance and insulin sensitivity were not increased (Extended Data Fig. 8o,p). Constitutively active GCGR overexpression significantly increased GPa and PEPCK enzyme activity (Extended Data Fig. 8y). These tests demonstrated that transiently increased exogenous expression of constitutively active GCGR increased hepatic glucose production. Furthermore, we observed weight reduction in three groups (the medium dosage AAV-*PvGCGR* (*PvGCGR_M*), *ScGCGR_M* and *ScGCGR_H* groups), with the largest weight reduction in the *ScGCGR_H* group (approximately 20% compared with the control group with high dosage injection of AAV-*HsGCGR* (*HsGCGR_H* group)) (Fig. 4c,d), despite significantly increased food intake in the *ScGCGR_H* group (Extended Data Fig. 8q,r). Oil Red O staining showed fewer lipid droplets in the livers of the *ScGCGR_M* group (Extended Data Fig. 9a). RT-qPCR and RNA-sequencing data showed an increase of genes involved in glycolysis and gluconeogenesis (*Pck1*, *Pck2* and *G6pc1*), lipolysis (*Lpl*) and energy metabolism (*Fgf21*) (Fig. 4f, Extended Data Figs. 8z, 9e–g and Supplementary Table 9), and correspondingly, lipogenesis genes (*Acc* and *Fasn*) were downregulated in the *ScGCGR_M* group (Extended Data Fig. 8s,aa). Serum NEFAs increased, whereas hepatic NEFAs and triglycerides decreased in the *ScGCGR_M* group (Extended Data Fig. 8t,u). No histopathological changes were observed in the liver or pancreas of all groups (Extended Data Fig. 9b–d).

To exclude the potential influence of endogenous mouse GCG on the regulatory effect of constitutively active GCGR in glucose and lipid

metabolism, we established GCG-knockout mice (Fig. 4h). We injected eight-week old GCG-knockout mice with the same dose as the *ScGCGR_M* group, resulting in a phenotype consistent with that shown in Fig. 4a–d. The mice exhibited increased blood glucose levels accompanied by reduced body weight (Fig. 4i). In addition to the upregulation of genes involved in glycogenesis (Fig. 4k), we found an increase in the expression of genes related to lipolysis and a decrease in the expression of genes associated with lipogenesis in the liver of these *ScGCGR_M* mice (Extended Data Fig. 8ab–ad). Finally, we constructed *ScGCGR* conditional knock-in (CKI-*ScGCGR*-Alb-iCre) mice. *ScGCGR* expression was lower compared with the AAV-*ScGCGR_H* mice, but we nevertheless observed a similar but less pronounced phenotype compared with that presented in Fig. 4a–d,h,i (Fig. 4l–o and Extended Data Fig. 8ae,af).

SNPs can help explain differences in susceptibility to diseases across a population. From an SNP database, we tested constitutive activities of mutant *HsGCGR* proteins. As established by transfection in HEK293 cells, the *HsGCGR*(H339R) variant exhibited weak constitutive activity, similar to that of *Petaurus breviceps* GCGR (*PbGCGR*) (Extended Data Fig. 10a). We synthesized an AAV for expression of *HsGCGR*(H339R) in mouse liver (Extended Data Fig. 10a–j). In the high-titre *HsGCGR*(H339R)_H group, we observed increased blood glucose and weight loss compared with control groups (*HsGCGR* and null) (Extended Data Fig. 10b,c). *Pck1* and *G6pc1* expression were also increased (Extended Data Fig. 10d) and GPa enzyme activity increased while hepatic glycogen content decreased (Extended Data Fig. 10e,f) in the *HsGCGR*(H339R)_H group compared with the control groups. Expression of the lipolysis gene *Lpl* increased, but no changes were observed in the expression of lipogenesis genes (*Acc*, *Acot7*, *Fasn*, *Pparg* and *Cebpa*) (Extended Data Fig. 10g,h) or in serum or hepatic triglycerides and NEFAs (Extended Data Fig. 10i,j). Mice in the *HsGCGR*(H339R)_H group exhibited a phenotype (high blood glucose) resembling that of mice injected with AAV-*ScGCGR* (Fig. 4a–c and Extended Data Fig. 10b). However, the AAV-*ScGCGR*-injected mice exhibited a more pronounced phenotype than the *HsGCGR*(H339R)_H mice (Fig. 4b–d,i,m).

As constitutively active GCGR resulted in body weight loss, we injected diet-induced obese (DIO) male mice (after 23 weeks of high-fat diet (HFD)) with high titres of AAV-*HsGCGR* (*HsGCGR_H* group), AAV-*ScGCGR* (*ScGCGR_H*) or null (Extended Data Fig. 10q–z). *ScGCGR_H* injection in liver (Extended Data Fig. 10s) resulted in a significant increase in blood glucose and weight loss (15% of initial weight) (Extended Data Fig. 10r) compared with the *HsGCGR_H* and null groups. RT-qPCR and RNA-sequencing data showed that expression of genes associated with glycolysis and gluconeogenesis (*G6pc1* and *Pck1*) and lipolysis (*Lpl*) increased, and correspondingly, expression of lipogenesis genes (*Acc* and *Fasn*) decreased (Extended Data Fig. 10v–z and Supplementary Tables 10, 11).

Avian GCGR leads to increased basal metabolism

The GCG–GCGR axis directly increases basal metabolism rate and energy expenditure by stimulating FGF21 secretion from extrahepatic tissues in rodents⁵⁰. Therefore, we further investigated the relationship between constitutive GCGR activity and basal metabolic rate in mice (Fig. 4p and Extended Data Fig. 11a). We found increased expression of *Fgf21* in liver in the *ScGCGR* group compared with null or *HsGCGR* groups, consistent with our RNA-sequencing, RT-qPCR (Fig. 4f and Extended Data Fig. 11a) and ex vivo (Extended Data Fig. 11d,e) data.

Indirect calorimetry analysis revealed that total oxygen consumption (VO_2) and carbon dioxide production (VCO_2) were significantly higher in the ScGCGR group than in the HsGCGR and null groups during both light and dark phases (Fig. 4p and Extended Data Fig. 11b). Correspondingly, energy expenditure was significantly increased in ScGCGR mice during both light and dark phases (Fig. 4p and Extended Data Fig. 11c). Furthermore, the basal metabolic rate of the birds *L. striata* and *M. undulatus* decreased following downregulation of GCGR (Fig. 4q,r). Similarly, 30-day-old chicks injected with AAV-shGcGCGR exhibited a largely decreased basal metabolic rate compared with those injected with AAV-shCtrl (Fig. 4s). Moreover, an increased basal metabolic rate was found in the gecko *E. macularius* injected with ScGCGR but not in the HsGCGR or null groups (Fig. 4t), and similar results were obtained in transgenic zebrafish (Fig. 4u). Thus, high expression of constitutively active GCGRs also affected basal metabolic rates, consistent with the observed differences in basal metabolic rate among vertebrates (Extended Data Fig. 11f,g and Supplementary Table 12).

Discussion

Exogenous GCG has previously been shown to markedly increase circulating glucose concentrations in chickens⁵¹. However, the GCG antagonist des-His¹(Glu⁹) glucagon amide does not alter blood glucose in fed chickens⁵². This is consistent with our observation that a GCGR antagonist, des-His¹Pro⁴-glucagon amide, did not affect blood glucose levels in chicks (Fig. 2a), suggesting that maintenance of high blood glucose in birds may not depend on ligand-mediated regulation.

GCGR from non-placental mammals has weak constitutive activity, whereas eutherian GCGR has no constitutive activity and is highly expressed in liver (Fig. 1d). By contrast, in most non-mammalian vertebrates, GCGR has high constitutive activity and is expressed at low levels in liver (Fig. 1d). Of the non-mammalian vertebrates that we tested, only Aves and Agamidae showed high GCGR expression in the liver (Fig. 1d and Extended Data Fig. 4). Constitutive GCGR activity was dependent on the interaction of the stalk, ECL1 and ICL2 regions (Extended Data Fig. 2 and Supplementary Figs. 2, 3). Knockdown of *GCGR* gene expression or inhibition of GCGR constitutive activity with the allosteric inhibitor adomeglivant resulted in downregulation of the carbohydrate metabolism pathway. By screening human SNP data, we identified HsGCGR(H339R), a naturally occurring variant with a point mutation in ICL3 that results in weak constitutive activity (Extended Data Fig. 10). High-titre injection of mice with an AAV construct for expression of HsGCGR(H339R) resulted in high expression in the liver and an avian-like phenotype, including high blood glucose and reduced body weight (Extended Data Fig. 10). The loss of constitutive GCGR activity in placental mammals may have countered disadvantages caused by excessive activation of GCGR signalling, such as the inability to manage energy expenditure when food is scarce. The function of non-constitutively active GCGRs is strictly regulated by ligand binding (Extended Data Fig. 1w–z). This allows precise signal transduction and regulation, enabling eutherian species to adapt to various external environments. By contrast, birds can utilize the energy provided by constitutively active GCGR for flight, and have presumably evolved other molecular and behavioural strategies (including migration) to manage environmental changes⁵³.

We suggest that constitutively active GCGR resembles a switch that is permanently, but only partially, on (Fig. 5 and Extended Data Fig. 12)—that is, it does not have a complete off switch but can be further activated by its ligand (Extended Data Fig. 1w–z) or expression levels (Fig. 1d and Extended Data Fig. 3b). In our study, *GCGR* maintains high hepatic expression of more than 8%, relative to β -actin, and consequently results in high blood glucose and basal metabolic rates in birds and Agamidae (Fig. 4q–t and Extended Data Figs. 3–5). Avian GCGR constitutively activates downstream G_s signalling, resulting in persistent glycogen metabolism, thereby stimulating gluconeogenesis and lipolysis to alter physiological functions, resulting in high

blood glucose, low body weight and high basal metabolic rate (Fig. 4 and Extended Data Figs. 8, 9). GCGR activity requires external energy input, which may be provided by increased food intake in our chow diet mouse model (Extended Data Fig. 8q,r). In contrast to vertebrates with high constitutive GCGR activity, non-placental mammals with weakly constitutively active GCGR, and eutheria, which lack constitutive GCGR activity, maintain relatively high GCGR expression in the liver (Fig. 1a–d and Extended Data Fig. 3).

As one of the most diverse extant vertebrate groups, birds have unique physiological adaptations and exaptations for flight—for example, feathers and low body weight in relation to size combined with strong muscles and high metabolic rate^{54,55}. As the main fuel for short-term flight of birds, glucose is likely to facilitate rapid carbohydrate energy supply during the take-off phase^{7,19–22,56,57}, and the high blood glucose supported by high expression and constitutive activity of GCGR (Figs. 2, 3) provides a large energy pool. These high blood glucose concentrations can quickly replenish muscle glycogen in preparation for the next take-off⁵⁶. Previous studies have found higher circulating glucose concentrations in Neognathae compared to the flightless ratites (Palaeognathae)¹³. The constitutive activity and hepatic expression levels of GCGR in Palaeognathae are low compared to those in flight-capable birds (Fig. 2b and Extended Data Fig. 1r). High GCGR expression also facilitates effective fat utilization in the liver, which makes flight more energy efficient (Fig. 4 and Extended Data Figs. 5, 6h–j). Compared with running mammals, flying birds make more use of lipids—which are used as an energy source for long-distance flight⁵⁷—because the energy density of fat (39.6 kJ g^{-1}) is far higher than that of other energy sources⁵⁶. High GCGR expression helps to reduce body weight, which also increases energy efficiency of flight (Fig. 4 and Extended Data Figs. 10, 11). GCGR expression levels in birds are associated with a high basal metabolic rate and the evolution of flight. Flight has a higher energy cost than swimming or running⁵⁸, and therefore requires a higher metabolic rate. Flightless birds have lower basal metabolic rate than flying birds⁵⁹. Our results are consistent with the high energy consumption rate required for sustained flapping flight⁶⁰ and with the occurrence of a major physiological shift towards a higher basal metabolic rate in birds compared with non-avian dinosaurs and reptiles as part of the adaptations and exaptations for flight⁶¹ (Fig. 4p–u and Extended Data Fig. 11). Thus, regulation of avian GCGR may have contributed to the adaptive flight physiology of birds to some extent by increasing blood glucose, fat utilization and basal metabolic rate (Fig. 5 and Extended Data Fig. 12). To adapt to new environments or challenges, organisms that evolved one such putative adaptation, such as high levels of *GCGR* transcription, in addition to the maintenance of ancestral constitutive activity, use additional ‘adjusting screws’ or ‘set screws’ to further enhance or counteract these effects, such as enhanced or reduced *GCGR* gene expression levels and many other (for example, downstream) mechanisms. In conclusion, constitutively active GCGR with high hepatic expression may underlie sustained high blood glucose in birds and contributed, among many other adaptations and exaptations, to the evolution of flight in birds and their ancestors.

Our study has some limitations. First, the structural basis of constitutive avian GCGR activity remains largely unexplored owing to the absence of a crystal structure⁶² and limited mutational coverage. Further studies are needed to examine structural differences between avian and eutherian GCGR. Second, the availability of tissue samples from various species was limited because of the regulations of the National Forestry and Grassland Administration of China, which constrained the breadth of species that we could examine. Third, the limited availability of GCGR sequences and tissue samples across bird species restricted our conclusions regarding the role of constitutively active GCGR in avian flight ability. Finally, as flight has evolved separately in different phyla, we cannot assume that identical molecular mechanisms and anatomical features evolved in parallel—bats, for example, did not evolve feathers for flight, and so the evolution of

flight in bats might not have involved GCGR regulation in the same way as in birds.

Online content

Any methods, additional references, Nature Portfolio reporting summaries, source data, extended data, supplementary information, acknowledgements, peer review information; details of author contributions and competing interests; and statements of data and code availability are available at <https://doi.org/10.1038/s41586-025-08811-8>.

- Irwin, D. M. Evolution of hormone function: proglucagon-derived peptides and their receptors. *BioScience* **55**, 583 (2005).
- Brubaker, P. L. & Drucker, D. J. Structure–function of the glucagon receptor family of G protein-coupled receptors: the glucagon, GIP, GLP-1, and GLP-2 receptors. *Recept. Channels* **8**, 179–188 (2002).
- Cardoso, J. C. R. et al. Evolution of the glucagon-like system across fish. *Gen. Comp. Endocrinol.* **264**, 113–130 (2018).
- Ng, S. Y. L., Lee, L. T. O. & Chow, B. K. C. Insights into the evolution of proglucagon-derived peptides and receptors in fish and amphibians. *Ann. NY Acad. Sci.* **1200**, 15–32 (2010).
- Polakof, S., Mommsen, T. P. & Soengas, J. L. Glucosensing and glucose homeostasis: From fish to mammals. *Comp. Biochem. Physiol. B* **160**, 123–149 (2011).
- Xiong, Y. & Lei, F. SLC2A12 of SLC2 gene family in bird provides functional compensation for the loss of SLC2A4 gene in other vertebrates. *Mol. Biol. Evol.* **38**, 1276–1291 (2020).
- Han, H.-S., Kang, G., Kim, J. S., Choi, B. H. & Koo, S.-H. Regulation of glucose metabolism from a liver-centric perspective. *Exp. Mol. Med.* **48**, e218 (2016).
- Braun, E. J. & Sweazea, K. L. Glucose regulation in birds. *Comp. Biochem. Physiol. B* **151**, 1–9 (2008).
- Röder, P. V., Wu, B., Liu, Y. & Han, W. Pancreatic regulation of glucose homeostasis. *Exp. Mol. Med.* **48**, e219 (2016).
- Langendorff, O. Versuche über die Pankreasverdauung der Vögel. *Arch. Physiol.* **10**, 1–35 (1879).
- Koppányi, T., Ivy, A. C., Tatum, A. L. & Jung, F. T. Studies in avian diabetes and glycosuria. *Am. J. Physiol.* **78**, 666–674 (1926).
- Minkowski, O. Untersuchungen über den Diabetes mellitus nach Exstirpation des Pankreas. *Archiv Experiment. Pathol. Pharmacol.* **31**, 85–189 (1893).
- Scanes, C. G. In *Sturkie's Avian Physiology* (eds Scanes, C. G. & Dridi, S.) 613–645 (Academic Press, 2022).
- Hauser, A. S., Attwood, M. M., Rask-Andersen, M., Schiöth, H. B. & Gloriam, D. E. Trends in GPCR drug discovery: new agents, targets and indications. *Nat. Rev. Drug Discov.* **16**, 829–842 (2017).
- Campos, R. V., Lee, Y. C. & Drucker, D. J. Divergent tissue-specific and developmental expression of receptors for glucagon and glucagon-like peptide-1 in the mouse. *Endocrinology* **134**, 2156–2164 (1994).
- Svoboda, M., Tastenoy, M., Vertongen, P. & Robberecht, P. Relative quantitative analysis of glucagon receptor mRNA in rat tissues. *Mol. Cell. Endocrinol.* **105**, 131–137 (1994).
- Richards, M. P. & McMurtry, J. P. Expression of proglucagon and proglucagon-derived peptide hormone receptor genes in the chicken. *Gen. Compar. Endocrinol.* **156**, 323–338 (2008).
- Petersen, M. C., Vatner, D. F. & Shulman, G. I. Regulation of hepatic glucose metabolism in health and disease. *Nat. Rev. Endocrinol.* **13**, 572–587 (2017).
- DeFronzo, R. A. Pathogenesis of type 2 diabetes mellitus. *Med. Clin. N. Am.* **88**, 787–835 (2004).
- Jiang, G. & Zhang, B. B. Glucagon and regulation of glucose metabolism. *Am. J. Physiol.* **284**, E671–E678 (2003).
- Mata-Torres, G., Andrade-Cetto, A., Espinoza-Hernández, F. A. & Cárdenas-Vázquez, R. Hepatic glucose output inhibition by Mexican plants used in the treatment of type 2 diabetes. *Front. Pharmacol.* **11**, 215 (2020).
- Rodgers, R. L. Glucagon and cyclic AMP: time to turn the page? *Curr. Diabetes Rev.* **8**, 362–381 (2012).
- Hayes, J. M. In *Discovery and Development of Antidiabetic Agents from Natural Products* 29–62 (Elsevier, 2017).
- Agius, L. Physiological control of liver glycogen metabolism: lessons from novel glycogen phosphorylase inhibitors. *Mini Rev. Med. Chem.* **10**, 1175–1187 (2010).
- Agius, L. Role of glycogen phosphorylase in liver glycogen metabolism. *Mol. Asp. Med.* **46**, 34–45 (2015).
- Hasegawa, K., Sakamaki, Y., Tamaki, M. & Wakino, S. PCK1 protects against mitochondrial defects in diabetic nephropathy in mouse models. *J. Am. Soc. Nephrol.* **34**, 1343–1365 (2023).
- Longuet, C., Sinclair, E. M., Maida, A., Baggio, L. L. & Drucker, D. J. Glucagon stimulates fatty acid oxidation and inhibits triglyceride synthesis in a PPAR α -, p38 MAPK- and AMPK-dependent manner. *Diabetes* **56**, A39–A40 (2007).
- Seifert, R. & Wenzel-Seifert, K. Constitutive activity of G-protein-coupled receptors: cause of disease and common property of wild-type receptors. *Naunyn Schmiedeberg's Arch. Pharmacol.* **366**, 381–416 (2002).
- Sveidahl Johansen, O. et al. Lipolysis drives expression of the constitutively active receptor GPR3 to induce adipose thermogenesis. *Cell* **184**, 3502–3518.e33 (2021).
- Tao, Y.-X. Constitutive activation of G protein-coupled receptors and diseases: insights into mechanisms of activation and therapeutics. *Pharmacol. Ther.* **120**, 129–148 (2008).
- Wifling, D. et al. Molecular determinants for the high constitutive activity of the human histamine H4 receptor: functional studies on orthologues and mutants. *Br. J. Pharmacol.* **172**, 785–798 (2015).
- Peeters, M. C. et al. Domains for activation and inactivation in G protein-coupled receptors – A mutational analysis of constitutive activity of the adenosine A_{2b} receptor. *Biochem. Pharmacol.* **92**, 348–357 (2014).
- El Khamlichi, C., Cobret, L., Arrang, J.-M. & Morisset-Lopez, S. BRET analysis of GPCR dimers in neurons and non-neuronal cells: evidence for inactive, agonist, and constitutive conformations. *Int. J. Mol. Sci.* **22**, 10638 (2021).
- Killion, E. A. et al. Chronic glucose-dependent insulinotropic polypeptide receptor (GIPR) agonism desensitizes adipocyte GIPR activity mimicking functional GIPR antagonism. *Nat. Commun.* **11**, 4981 (2020).
- Shao, L. et al. Modulating effects of RAMPs on signaling profiles of the glucagon receptor family. *Acta Pharm. Sin.* **B 12**, 637–650 (2022).
- Wang, T., Hung, C. C. Y. & Randall, D. J. The comparative physiology of food deprivation: from feast to famine. *Annu. Rev. Physiol.* **68**, 223–251 (2006).
- Edwards, M. R., McMurtry, J. P. & Vasilatos-Younken, R. Relative insensitivity of avian skeletal muscle glycogen to nutritive status. *Domest. Anim. Endocrinol.* **16**, 239–247 (1999).
- Kamesh, N., Aradhya, G. K. & Manoj, N. The repertoire of G protein-coupled receptors in the sea squirt *Ciona intestinalis*. *BMC Evol. Biol.* **8**, 129 (2008).
- Qiao, A. et al. Structural basis of G_s and G_i recognition by the human glucagon receptor. *Science* **367**, 1346–1352 (2020).
- Siu, F. Y. et al. Structure of the human glucagon class B G-protein-coupled receptor. *Nature* **499**, 444–449 (2013).
- Zhang, H. et al. Structure of the full-length glucagon class B G-protein-coupled receptor. *Nature* **546**, 259–264 (2017).
- Holmes, D. J., Flückiger, R. & Austad, S. N. Comparative biology of aging in birds: an update. *Exp. Gerontol.* **36**, 869–883 (2001).
- Polakof, S., Panserat, S., Soengas, J. L. & Moon, T. W. Glucose metabolism in fish: a review. *J. Comp. Physiol. B* **182**, 1015–1045 (2012).
- Zhang, H. et al. Structure–activity relationship and conformational studies of the natural product cyclic depsipeptides YM-254890 and FR900359. *Eur. J. Med. Chem.* **156**, 847–860 (2018).
- Morrison, J. K. et al. Single-cell transcriptomics reveals conserved cell identities and fibrogenic phenotypes in zebrafish and human liver. *Hepatol. Commun.* **6**, 1711–1724 (2022).
- Liao, Y. et al. Cell landscape of larval and adult *Xenopus laevis* at single-cell resolution. *Nat. Commun.* **13**, 4306 (2022).
- Su, Q. et al. Single-cell RNA transcriptome landscape of hepatocytes and non-parenchymal cells in healthy and NAFLD mouse liver. *iScience* **24**, 103233 (2021).
- Payen, V. L. et al. Single-cell RNA sequencing of human liver reveals hepatic stellate cell heterogeneity. *JHEP Rep.* **3**, 100278 (2021).
- Zeng, L. et al. Contribution of gene regulatory networks to heritability of coronary artery disease. *J. Am. Coll. Cardiol.* **73**, 2946–2957 (2019).
- Kim, T. et al. Glucagon receptor signaling regulates energy metabolism via hepatic farnesoid X receptor and fibroblast growth factor 21. *Diabetes* **67**, 1773–1782 (2018).
- Ruffier, L., Simon, J. & Rideau, N. Isolation of functional glucagon islets of Langerhans from the chicken pancreas. *Gen. Comp. Endocrinol.* **112**, 153–162 (1998).
- Simon, J., Derouet, M. & Gespach, C. An anti-insulin serum, but not a glucagon antagonist, alters glycemia in fed chickens. *Horm. Metab. Res.* **32**, 139–141 (2000).
- Winkler, D. W. et al. Cues, strategies, and outcomes: how migrating vertebrates track environmental change. *Mov. Ecol.* **2**, 10 (2014).
- Bundle, M. W., Hoppeler, H., Vock, R., Tester, J. M. & Weyand, P. G. High metabolic rates in running birds. *Nature* **397**, 31–32 (1999).
- Hedenström, A. Adaptations to migration in birds: behavioural strategies, morphology and scaling effects. *Phil. Trans. R. Soc. B* **363**, 287–299 (2008).
- Butler, P. J. The physiological basis of bird flight. *Phil. Trans. R. Soc. B* **371**, 20150384 (2016).
- Bishop, C. M. & Guglielmo, C. G. In *Sturkie's Avian Physiology* (eds Scanes, C. G. & Dridi, S.) 1265–1329 (Academic Press, 2022).
- Schmidt-Nielsen, K. Locomotion: energy cost of swimming, flying, and running. *Science* **177**, 222–228 (1972).
- Ballesteros, F. J. et al. On the thermodynamic origin of metabolic scaling. *Sci. Rep.* **8**, 1448 (2018).
- Wingfield, J. C. In *Sturkie's Avian Physiology* (eds Scanes, C. G. & Dridi, S.) 3–6 (Academic Press, 2022).
- Li, Q. et al. Melanosome evolution indicates a key physiological shift within feathered dinosaurs. *Nature* **507**, 350–353 (2014).
- Behan, D. P. & Chalmers, D. T. The use of constitutively active receptors for drug discovery at the G protein-coupled receptor gene pool. *Curr. Opin. Drug Discov. Dev.* **4**, 548–560 (2001).

Publisher's note Springer Nature remains neutral with regard to jurisdictional claims in published maps and institutional affiliations.



Open Access This article is licensed under a Creative Commons Attribution-NonCommercial-NoDerivatives 4.0 International License, which permits any non-commercial use, sharing, distribution and reproduction in any medium or format, as long as you give appropriate credit to the original author(s) and the source, provide a link to the Creative Commons licence, and indicate if you modified the licensed material. You do not have permission under this licence to share adapted material derived from this article or parts of it. The images or other third party material in this article are included in the article's Creative Commons licence, unless indicated otherwise in a credit line to the material. If material is not included in the article's Creative Commons licence and your intended use is not permitted by statutory regulation or exceeds the permitted use, you will need to obtain permission directly from the copyright holder. To view a copy of this licence, visit <http://creativecommons.org/licenses/by-nc-nd/4.0/>.

© The Author(s) 2025

Methods

Plasmids and transfection

GCCR genes were synthesized by General Biology System and inserted into pcDNA3.1-n-Flag-His vector. The GCCR sequences of different species are shown in Supplementary Table 2. GCCR mutants were generated by site-directed mutagenesis using the QuikChange mutagenesis protocol (Agilent Technologies). Ten million cells were transfected with 0.2 µg of each plasmid of interest.

Cell lines

HEK293, AML12 and HEK293T cells were obtained from National Collection of Authenticated Cell Cultures (Chinese Academy of Sciences). HEK293 and HEK293T cells were cultured in Dulbecco's Modified Eagle Medium (DMEM, Gibco) supplemented with 10% fetal bovine serum and 100 IU ml⁻¹ penicillin and 100 µg ml⁻¹ streptomycin and incubated at 37 °C in a humidified 5% CO₂ incubator. AML12 cells were cultured in complete medium (CM-0602, Procell Life Science & Technology), and incubated at 37 °C in a humidified 5% CO₂ incubator. LMH cells (chicken hepatocellular carcinoma epithelial) were obtained from American type culture collection (ATCC, CRL-2117) cultured in Dulbecco's Modified Eagle Medium (DMEM/F-12, Gibco) supplemented with 10% fetal bovine serum and 100 IU ml⁻¹ penicillin and 100 µg ml⁻¹ streptomycin and incubated at 39 °C in a humidified 5% CO₂ incubator.

Chemicals and peptides

H89, YM254890 and adomeglivant were purchased from MedChemExpress (MCE). GCG, GLP1, GLP2, GCGL, GIP and des-His¹Pro⁴-glucagon amide were synthesized by GL Biochem. All peptides were > 95% pure. Peptide sequences are organized in Supplementary Table 13.

Animals

C57BL/6 J (wild type and DIO) and *db/db* (a diabetes model with a mutation in the leptin receptor gene *Lepr*) were purchased from GemPharmatech. Mice were housed under conventional conditions in filter-top protected cages and cared for in accordance with the Experimental Animal Laboratory Center of West China Hospital. Food and water were provided ad libitum. Specific pathogen-free (SPF) chickens were purchased online (<http://www.bosgene.com.cn>). *L. striata*, *Melopsittacus undulatus*, *Chrysemys picta picta*, *Rana catesbeiana* Shaw, *Rana nigromaculata* and *D. rerio* were purchased online (<https://www.taobao.com/>). *Xenopus tropicalis* was purchased online (<http://www.xenopus.cn/>). A GgGCCR transgenic zebrafish line was constructed and raised at Nanjing Xinjia Medical Technology. All animals involved in this study were listed on Supplementary Table 3.

All mice were maintained on a 12/12 h day/night cycle, an average ambient temperature of 22 °C and an average humidity of 48% at 5 animals per cage and provided food and water ad libitum. One- to two-year-old budgerigars (*M. undulatus*) (green base color, yellow-green body feathers, black or dark brown stripes on the head, neck and back, medium body size), white-rumped Munia (*L. striata*) (black face, brown back and wings, white belly and waist, medium body size) were maintained on a regular 12/12 h day/night cycle at five adult birds per cage (160 cm × 50 cm × 40 cm, length × height × width). Ambient temperature of the vivarium was maintained between 21 to 23 °C and average humidity was maintained 48%. The cages were made of white metal bars, and each contained a long-suspended perch, with feeders placed below the perch to provide water and food (ad libitum). Chickens were kept free-range in a chicken coop with an area of 5 m × 10 m on a 16/8 h day/night cycle, an average ambient temperature of 23 °C and an average humidity of 60%. The coop has a 16/8 light/dark cycle, with an exhaust fan installed to maintain proper air circulation inside the coop. The water dispenser provides water

continuously, and the feed trays are refilled with food twice a day at scheduled times. The floor is cleaned and disinfected regularly every day. Chick temperature management: For chicks under 1 week old, the temperature is maintained at 34–36 °C. Subsequently, the temperature is reduced by 2 °C each week until it reaches around 22–24 °C. The bearded dragon (*P. vitticeps*) and leopard gecko (*E. macularius*) are kept in a spacious enclosure with dimensions of 200 cm × 60 cm × 60 cm (length × height × width). The enclosure is lined with sand, and some stones and driftwood are placed inside. The enclosure is equipped with a thermometer and a heating lamp to maintain a temperature range of 28 to 32 °C, 10/14 light/dark cycle. Feeding occurs twice a day. The primary diet includes insects such as locusts and *Blaptica dubia*, and occasionally some vegetable and fruit including lettuce leaves. The bedding is regularly changed to maintain dryness and ventilation within the enclosure. Zebrafish were kept at 28 ± 0.5 °C in a ventilated recirculating tank with 14/10 light/dark cycle. Zebrafish larvae were fed paramecium twice daily. After 3–4 weeks krill was fed twice daily.

Blood and liver tissue samples

Macaca mulatta liver and blood samples were obtained from the Key Laboratory of Transplant Engineering and Immunology (West China Hospital, Sichuan University, China). The Natural Museum of Sichuan University provided blood and liver samples from *Phylloscopus magnirostris*, *Muscicapa ferruginea*, *Parus monticolus*, *Passer domesticus* and *Carpodacus vinaceus*. Fresh mammalian tissue samples (*Capra hircus*, *Sus scrofa* and *Bos taurus*) were purchased from Nanjing Zhushun Biotechnology. *Crocodylus siamensis* samples were purchased from Lvyan Crocodile Breeding.

Phylogenetic analysis of the GCG receptor family

Coding region sequences of GCCR were aligned by TranslatorX which is a perl program with default parameters. Unrooted phylogenetic tree was conducted by FastTree v2.1 based on the multiple alignment sequences.

cAMP and IP1 accumulation assays

cAMP and IP1 accumulation in HEK293 cells were measured using the cAMP HTRF kit and IP1 HTRF kit (Cisbio Bioassays–PerkinElmer), respectively, in accordance with the manufacturer's instructions. In brief, transfected HEK293 cells were seeded in a 96-well plate, and 36 h after transfection, cryptate-labelled anti-cAMP or anti-IP1 monoclonal antibody, and d2-labelled cAMP or IP1 in lysis buffer were added to the wells. After 1 h of incubation at room temperature, the plates were read in EnVision Multilabel Plate Reader with excitation at 337 nm and emission at 620 and 665 nm. The accumulation of cAMP or IP1 was calculated according to the HTRF ratio (665 nm/620 nm).

Luciferase assays

To detect constitutive activity of GCCR, HEK293 cells were seeded in 96-well plates and co-transfected with the luciferase reporter genes including CRE, nuclear factor of activated T-cells response element (NFAT-RE), serum response factor response element (SRF-RE, a mutant form of SRE) and serum response element (SRE) were utilized for testing G_s, G_q, G₁₂ and potential G_i signalling⁶³, respectively, and other potential signalling (MYC, p53, ISRE, NF-κB, AP-1 and GLI)⁶⁴. Twenty-four hours after transfection, cells were further incubated with various ligands from different species, diluted by serum-free media for 12 h. Luciferase activities were determined using luciferase assay kits (Yeasen) by a EnVision Multilabel Plate Reader (PerkinElmer). All experiments were performed at least three times in triplicates. The fold was calculated compared to control.

For promoter activity assays, LMH cells (chicken hepatocellular carcinoma epithelial) were cultured to 70–80% in 24-well plates and

co-transfected with 500 ng of the reporter constructs and 10 ng of Renilla luciferase reporter vector pGL4.73 (Promega) as an expression control using Lipo3000 (Invitrogen).

Quantification of receptor expression in cells by ELISA

Thirty-six hours after transfection, HEK293 cells were fixed with 4% paraformaldehyde (PFA) and blocked with 1% FBS (blocking buffer). Cells were incubated for 30 min with primary antibody (HRP anti-Flag, 1:1,000; Sigma). After twice washing with the blocking buffer and phosphate-buffered saline each, HRP signal was quantified by chemiluminescence with SuperSignal substrate (New Cell & Molecular Biotech) and an EnVision Multilabel Plate Reader (PerkinElmer).

RNA purification, cDNA synthesis and RT-qPCR

Total RNA was isolated using TRIzol Reagent (CWBio), according to the manufacturer's instructions. RNA was converted to cDNA using HiScript III RT SuperMix for RT-PCR (Vazyme). Quantitative PCR reactions were prepared using ChamQ Universal SYBR RT-qPCR Master Mix (Vazyme). All reactions were performed in triplicate. The RT-qPCR amplification steps: 95 °C 1 min; 45 cycles of 95 °C 5 s and 60 °C 30 s. RNA abundance was normalized to an endogenous reference gene (β -actin) and calculated as delta threshold cycle (Δ Ct). The RT-qPCR targets were normalized to the expression of the β -actin gene. Primer sequences for RT-qPCR are provided in Supplementary Table 14.

Nuclei preparation

Nuclei were isolated using a Nucleus Isolation Kit (SHBIO 52009-10) as instructed by the manufacturer. RNase inhibitors (Sigma 3335399001) were added to the reagents before use. The samples were cut and transferred to a 5 ml tube containing lysate, mixed and lysed for 3 min on ice, then filtered through a 40- μ m cell filter (Sigma BAH136800040). Nuclei count and viability were estimated using fluorescence Cell Analyzer (Countstar Rigel S2) with AO/PI reagent. The nuclei were stained with 0.4% trypan blue and placed under a microscope (40 \times). Subsequent experiments were performed when the nuclear envelope was intact and there were few impurities.

snRNA-seq sequencing library construction and sequencing

snRNA-seq libraries were prepared using SeekOne Digital Droplet Single Cell 3' library preparation kit (SeekGene, K00202). In brief, appropriate number of cell nucleus were mixed with reverse transcription reagent and then added to the sample well in SeekOne DD Chip S3. Subsequently, Barcoded Hydrogel Beads (BHBs) and partitioning oil were dispensed into corresponding wells separately in chip S3. After emulsion droplet generation reverse transcription were performed at 42 °C for 90 min and inactivated at 80 °C for 15 min. Next, cDNA was purified from broken droplets and amplified in a RT-qPCR reaction. The amplified cDNA product was then cleaned, fragmented, end repaired, A-tailed and ligated to sequencing adaptors. Finally, the indexed PCR was performed to amplify the DNA representing the 3' polyA part of RNAs, which also contained the cell barcode and unique molecular index (UMI). The indexed sequencing libraries were cleaned with SPRI beads, quantified by quantitative PCR (KAPA Biosystems KK4824) and then sequenced on illumina NovaSeq 6000 with PE150 read length.

Sequencing data quality control

Fastp was used to trim primer sequences and low-quality bases of raw reads and collect the basic statistics collected. The specific parameters could be summarized as below: (1) A 1-bp sliding window was moved from tail (3') to front. The bases in the window were dropped if their mean quality was below 3, and the window kept moving until the last base. The trailing N bases were also trimmed, similar to the Trimmomatic TRAILING method; (2) The auto adapter was detected for PE data;

(3) Trimmed reads shorter than 60 bp were discarded. The cleaned reads after trimming were used in the following steps.

Processing the snRNA-seq data

We used the SeekSoul Tools pipeline to process the cleaned reads and generated the transcript expression matrix. First, the cell barcodes and UMI sequences were extracted based on the defined pattern about the localization of the barcode, linker and UMI within a read. The barcode was corrected with whitelist. The corrected barcode, together with UMI, were put in the header of their corresponding reads. Second, the reads were mapped to the reference genomes using STAR 2.5.1b. Then, the reads with barcode and UMI information were assigned to the transcriptome using featureCounts of package Subread 1.6.4. Finally, similar to the raw_feature_bc_matrix results of Cell Ranger, the raw UMI count matrix according to barcodes and transcripts was generated. A cell-calling algorithm was used to filter the raw UMI count matrix and get the cell only filtered_feature_bc_matrix was obtained. The algorithm was similar to that of Cell Ranger and EmptyDrops, which had two key steps: (1) It used a cutoff based on total UMI counts of each barcode to identify cells. This step identified the primary mode of the high RNA content cells. (2) Then the algorithm used the RNA profile of each remaining barcode to determine if it is an 'empty' or a cell-containing partition. This step captured the low RNA content cells who's total UMI counts might be similar to the empty wells.

Cross-species integration, clustering, visualization and differential expression

Integration, clustering, visualization, and differential expression analysis were performed using Seurat. To compare cellular profiles with other species, the expression data matrix of liver from *M. undulatus*, *X. laevis*, *M. musculus* and *H. sapiens* were collected and re-analysed using the same criteria. We first generated homologous genes of *M. undulatus*, *X. laevis*, *M. musculus* and *H. sapiens* through Orthofinder (Version 2.5.4). We considered one-to-one orthology from all species. In order to compare and analyse liver cell profiles from all species mentioned, we used canonical correlation analysis to integrate their data as anchor datasets with dims = 1:40 for batch correction. Based on the shared structure, all batches of data were finally pooled into a single object for downstream analysis.

For clustering, 2,000 variable genes were used, and mitochondrial genes were removed from the variable gene set before running principal components analysis and calculating clusters using 20 principal components, and a resolution of 0.6. The nonlinear dimensional reduction technique was used to visualize and explore these datasets. We used the Wilcoxon rank sum test to find differential expression. We identified DEGs by the following criteria: (1) P value ≤ 0.05 ; (2) \log_2 (fold change) ≥ 0.2 ; and (3) the percentage of cells where the gene is detected in a specific cluster $>10\%$.

SAMap-based integration of *M. undulatus* and all data from other species

For the SAMap analysis⁶⁵ we first constructed BLAST maps among published proteomes of all species (*D. rerio*, *X. laevis*, *M. undulatus*, *M. musculus* and *H. sapiens*) with the default pipeline parameters (-max_hsp1, -evalue 1e-6). To integrate all species data using SAMap, we first converted Seurat objects with *M. undulatus* liver and published data (*D. rerio*⁴⁵, *X. laevis*⁴⁶, *M. undulatus*, *M. musculus*⁴⁷ and *H. sapiens*⁴⁸) to anndata objects using the R package loom. The anndata objects were then loaded into SAMap and processed with user-specified clusters ('Cell_Type' for all species) to determine neighbourhood sizes (neigh_from_keys = {'Dr':True, 'Xl':True, 'Ps':True, 'Mu':True, 'Mm':True, 'Hs':True}). To plot UMAPs, all Cell_Type from other species were transferred to human data by using SAMaps 'transfer_annotations'-function, all results were visualized by Scanpy (v1.9.1).

DEGs and KEGG enrichment analysis

Genes usually interact with each other to have roles in certain biological functions. Pathway-based analysis helps to further understand biological gene functions. Kyoto Encyclopedia of Genes and Genomes (KEGG) (<https://www.kegg.jp/>) pathway enrichment analysis identified significantly enriched metabolic pathways or signal transduction pathways in DEGs comparing to the whole genome background. Taking P value ≤ 0.05 as a threshold, pathways meeting this criterion were defined as significantly enriched pathways in DEGs.

ADV and AAV production

ADV constructs encoding the *GCGR* genes from the species of interest were produced and provided by Hanbio Biotechnology.

Recombinant AAV serotype 2/8 vectors that overexpress GCGR genes with a V5 tag (pAAV-CAG-GCGR-V5 tag-tWPA) were constructed by Shanghai Genechem.

For *GCGR* genes knockdown in hepatocytes of *M. undulatus*, *G. gallus*, *L. striata* and *P. vitticeps*, AAV serotype 2/9 vectors carrying shRNA (pAAV-U6-shRNA (GCGR)-CMV-EGFP-WPRE) were used. AAV-scramble shRNA-GFP was used as control (Genechem). The shGCGR sequences are provided in Supplementary Table 14.

Intravenous injection

For direct ADV- and AAV-mediated gene transfer into the liver, adult male C57BL/6 J mice were injected as previously described^{66–68}. ADV was injected into the tail vein of mice (1×10^{10} viral genomes (vg) per mouse). AAV2/8 displays a specific tissue tropism depending on the administration route. Intravenous injection into the tail vein of mice (low dosage: 1×10^{10} , medium dosage: 1×10^{11} , and high dosage 5×10^{11} vg per mouse) led to primarily liver transduction.

For chicken embryo endogenous *GCGR* gene interference experiments, fertilized chicken eggs at 15 days after laying were selected. Under sterile conditions, embryos were vein injected with AAV-shGCGR (2×10^{11} vg per individual) after breaking the shells and further incubated.

For *G. gallus* and *L. striata* interference experiments, we injected AAV-sh(GCGR) (2×10^{11} vg per individual) under the wings separately.

For budgerigar endogenous *GCGR* gene interference experiments, we injected AAV 2/9-CAG-shGCGR (2×10^{11} vg per individual) into budgerigar axillary veins after local wing hair removal under sterile conditions.

Local virus delivery in reptiles

Experimental animals were injected with AAV8 vector (2×10^{10} vg particles) carrying ScGCGR or HsGCGR.

Blood glucose measurement, GTT and ITT

General blood glucose measurements were done in various species fed ad libitum. For glucose tolerance test (GTT) and insulin tolerance test (ITT), seven days after transduction of AAV, mice were fasted overnight and GTT was performed. For ITT mice were fasted for 4 h before the experiment. Fasted mice were intraperitoneally injected with glucose 1.2 g kg^{-1} or insulin 0.75 U kg^{-1} body weight, respectively. Tail vein blood glucose was determined at time points 0, 15, 30, 60, 90 and 120 min using an automatic blood glucose meter (Roche).

Biochemical analysis

The amount of glycogen in liver and AML12 were quantified using a glycogen content assay kit (Solarbio) according to the manufacturer's instructions. Mouse serum was obtained by centrifugation at 3,000 rpm, and used for determining blood glucagon content according to manufacturer's instruction and for ELISA (R&D systems). Glucagon values are presented in pg ml^{-1} . Plasma insulin concentrations were measured by ELISA. Insulin ELISA kit (Mercodia) was used according to the manufacturer's instructions. Insulin values are presented in $\mu\text{g l}^{-1}$. GPa enzyme activation in AML12 and tissue samples were measured

using the Glycogen Phosphorylase a (GPa) Assay Kit (Solarbio) according to the manufacturer's instructions.

After fasting overnight for about 12 h, 500–800 μl blood was collected from mouse retro-orbital blood. The samples were placed at 4°C for 1–2 h and then centrifuged at 3,000 rpm at 4°C for 30 min. A fully automatic biochemical analyser (AU680, Beckman Coulter) was used with matching reagent kits. Serum levels of total bile acid (TBA), triglycerides and NEFA were measured according to the manufacturer's instructions.

The triglycerides assay kit were purchased from Beijing Leadman Biochemistry. The free fatty acids (NEFA) assay kit was purchased from Guangzhou Kofa Biotechnology.

Western blot analysis

For Western blot analysis, liver proteins were lysed by SDS (Beyotime) supplemented with proteinase inhibitor (Sparkjade). Protein concentration was measured using the BCA Protein Assay Kit (Sigma-Aldrich). Equal amounts of protein or sample were fractionated on a 10% SDS-PAGE gel and then transferred to a PVDF membrane (Bio-Rad). The blot was visualized using High Sensitivity ECL Kit (New Cell & Molecular Biotech). Primary antibodies, GCGR (1:1,000, Gene Universal), β -actin (1:1,000, Abways) were used in the experiments, HRP Anti-DDDDK tag (1:1,000, Abcam, UK). Secondary antibody (anti-rabbit horseradish peroxidase (HRP), 1:1,000; Abways).

Histological staining and immunofluorescence staining

Two tissue specimens were taken from each source: one was fixed in 4% formaldehyde/phosphate-buffered saline for more than 12 h for haematoxylin and eosin staining; the other specimen was cryosectioned for Immunofluorescence staining. Frozen sections were placed in a 37°C oven for 10–20 min to remove moisture and treated in fixative for 30 min. Sections in PBS (pH 7.4) were placed on a decolorizing shaker for 3 times, each for 5 min. After slightly drying the sections, the tissue was circled with a histochemical pen, then incubated with HCS LipidTOX Deep Red neutral lipid stain (H34477, Thermo). After deparaffinization, heat-induced antigen retrieval of dehydrated sections of tissue was performed by heating at 95°C in citrate buffer (pH 6.0) for 40 min, cooling to room temperature, and sealing in 5% normal goat serum. The sections were then incubated with the primary antibody, or anti-v5 (1:200, CST), or anti-insulin (1:200, Abcam), or anti-glucagon (1:200, CST) at 4°C overnight, then washed with PBS and incubated with second antibody (Alexa Fluor 488 conjugated Anti-rabbit IgG, 1:200, CST) at room temperature for 60 min. After washing with phosphate-buffered saline, the sections were mounted with Vectashield mounting medium containing DAPI ($10 \mu\text{g ml}^{-1}$, Vector Labs). Olympus VS200 and IXpolre SpinSR were used for section viewing and imaging (Evident, formerly Olympus Life Science Division).

Indirect calorimetry

An indirect open circuit calorimeter (TSE Systems) and air samples were analysed with a high-speed Siemens Ultramat/Oxymat 6 O_2/CO_2 analyser (TSE) as previously described^{69–71}. *M. musculus*, *M. undulatus* (one per cage) were acclimated to the metabolic chambers for 24 h, and data were collected in each cage every 27 min, during a 48-hour period. *G. gallus*, *L. striata* and *E. macularius* using a FoxBox Respirometry System as previously described⁷². The temperature during the measurement of *E. macularius* was controlled at 22°C . VO_2 (ml h^{-1}) and VCO_2 (ml h^{-1}) were calculated by TSE software, using the reference cage as measurement of (adjusted) oxygen and carbon dioxide inflow, and used to calculate the RER ($\text{RER} = \text{VCO}_2/\text{VO}_2$) and EE ($\text{EE} = (3.941 \times \text{VO}_2 + 1.106 \times \text{VCO}_2)/1,000$ in kcal min^{-1}). Samples were taken during light and dark cycles and were adjusted by lean body weight.

Zebrafish metabolism measurements

Animal metabolic rates were measured in an intermittent-closed swim tunnel respirometer with a swimming chamber measuring

14 × 14 × 55 cm (32.4 l water volume, Model 32, Loligo Systems). The swim tunnel was submerged into a water bath that served as a water reservoir for flushing the respirometer after each closed respirometer run (flush pump: Eheim, 38 l min⁻¹).

Oxygen saturation within the respirometer was measured using a Microx TX3 single channel oxygen meter (PreSens-Precision Sensing), equipped with a needle type fibre-optical micro-sensor (NTH, PreSens-Precision Sensing), suspended into the water current within the respirometer.

Measurements were performed in a sealed chamber of known volume (a closed respirometer). The oxygen content of the water is measured initially (t_0), then the respirometer is closed and at the end of the experiment (t_1) the oxygen content is measured again. Knowing the body weight of the animal (BW), the respirometer volume (V), and the oxygen content ($[O_2]$) of the water at time t_0 and t_1 , the mass specific oxygen consumption rate can be calculated as follows:

$$VO_2 = ([O_2]t_0 - [O_2]t_1) \times \frac{V}{t} \times \frac{1}{BW}$$

where VO_2 is the volume of oxygen and t is the measurement time.

Cumulative food intake, water intake and body weight

For cumulative food intake, cumulative water intake and body weight, ADV or AAV-injected mice were housed five per cage and the amount of diet consumed was recorded every two days at the same time of the day.

Analysis of gene expression levels

In order to calculate the GCGR expression levels in various animals, RNA-sequencing datasets were downloaded from the Sequence Read Archive (SRA). These data were generated from liver tissues of *C. hiriscus*, *Phascolarctos cinereus*, *G. gallus*, *Anas platyrhynchos*, *S. canaria*, *Zonotrichia albicollis*, *Microcaecilia dermatophaga*, *Lepisosteus oculatus*, *D. rerio* and *Ictalurus punctatus*.

FastQC (<http://www.bioinformatics.babraham.ac.uk/projects/fastqc/>) was used for quality control checks with the above data, according to the above results to trim low-quality reads using Trimmomatic⁷³. Hisat2⁵⁰ was applied with the default command options to align the trimmed reads against the reference genome. Finally, featureCounts⁷⁴ was used to count the reads aligned to each gene. The transcripts per million reads (TPM) was calculated using R in our study to quantify the gene expression levels.

Selection for chickens

The chicken breed was the Chinese yellow-feathered broiler, provided by Guangdong Wens Nanfang Poultry Breeding. Three hundred broilers about 40 days of age were randomly selected from the farm (male:female ratio ≈ 1:1) as the base population F_0 . The diet was a typical maize–soybean feed, containing 18% crude protein, 5.5% crude fibre, and 1,000 U kg⁻¹ phytase. Photoperiod was 15 h light:9 h dark for chickens less than 40 days of age or during the laying period, and 10 h light:14 h dark outside the laying period. Blood glucose was tested in chickens using an Accu-Chek Active Blood Glucose Meter (Roche) by collecting venous blood from the underside of the wings. The LG (low glucose) and HG (high glucose) lines of F_1 were established by 9 males and 39 females with the lowest mean blood glucose and the 2 males and 8 females with the highest average blood glucose of the F_0 generation at day 60 and 90 of age. Each male was mated to 4–5 females. The LG line of F_1 was divided into two groups bearing G/G or G/C for the establishment of F_2 lines, according to whether the G291C site was mutated.

Statistical analysis

Statistical analyses were performed on at least three individual datasets and analysed using GraphPad Prism software (v.10.2.0). Data are mean ± s.e.m. from at least three independent experiments, performed

in triplicates. Statistical significance was defined as: one-way ANOVA was used for comparisons between three groups, two-way repeated measures ANOVA was used for repeated measures data, and Student's t -test was used for comparisons between two groups. For dose–response experiments, data were normalized and analysed using nonlinear curve fitting for the log (agonist) versus response (three parameters) curves. ANCOVA was performed in R (version 4.4.0). The R package mainly included multcomp (version 1.4-26). The exact value of n (number of biological or experimental replicates) can be found in the figure legends and Supplementary Table 15.

Ethics statement

All animal care and experimental procedures complied with the Animal Management Regulations of the Ministry of Health, China (document no. 55, 2001) and were approved by the Science and Technology Department of Jiangsu Province (IACUC-20231210).

Reporting summary

Further information on research design is available in the Nature Portfolio Reporting Summary linked to this article.

Data availability

The snRNA-seq and bulk RNA-sequencing datasets have been deposited in the NCBI database under accessions PRJNA1209237 and PRJNA1211354. Publicly available datasets and databases used were the following: snRNA-seq data for *D. rerio*: GSE181987, *X. laevis*: GSM6214275, GSM6214276, *M. musculus*: GSE166504 and *H. sapiens*: GSE158723 (<https://www.ncbi.nlm.nih.gov/>). Naturally occurring GCGR mutations were registered in the gnomAD database v.2.1.1.

63. Cheng, Z. et al. Luciferase reporter assay system for deciphering GPCR pathways. *Curr. Chem. Genomics* **4**, 84–91 (2010).
64. Sarrion-Perdigones, A. et al. Examining multiple cellular pathways at once using multiplex hexuple luciferase assaying. *Nat. Commun.* **10**, 5710 (2019).
65. Tarashansky, A. J. et al. Mapping single-cell atlases throughout Metazoa unravels cell type evolution. *eLife* **10**, e66747 (2021).
66. Nason, S. R. et al. Glucagon-receptor signaling regulates weight loss via central KLB receptor complexes. *JCI Insight* **6**, e141323 (2021).
67. Nan, Y.-M. et al. Adenovirus-mediated peroxisome proliferator activated receptor gamma overexpression prevents nutritional fibrotic steatohepatitis in mice. *Scand. J. Gastroenterol.* **46**, 358–369 (2011).
68. Rodríguez-Márquez, E., Meumann, N. & Büning, H. Adeno-associated virus (AAV) capsid engineering in liver-directed gene therapy. *Expert Opin. Biol. Ther.* **21**, 749–766 (2021).
69. Angilletta, M. J. Jr & Angilletta, M. J. Jr Variation in metabolic rate between populations of a geographically widespread lizard. *Physiol. Biochem. Zool.* **74**, 11–21 (2001).
70. Attané, C. et al. Apelin treatment increases complete fatty acid oxidation, mitochondrial oxidative capacity, and biogenesis in muscle of insulin-resistant mice. *Diabetes* **61**, 310–320 (2012).
71. Elias, I. et al. Adipose tissue overexpression of vascular endothelial growth factor protects against diet-induced obesity and insulin resistance. *Diabetes* **61**, 1801–1813 (2012).
72. Wohlgemuth, R. P., Haro, D. & Liwanag, H. E. M. Osmotic and metabolic responses to cold acclimation and acute cold challenge in a freeze avoidant lizard, *Podarcis siculus*. *Comp. Biochem. Physiol. A* **283**, 111471 (2023).
73. Bolger, A. M., Lohse, M. & Usadel, B. Trimmomatic: a flexible trimmer for Illumina sequence data. *Bioinformatics* **30**, 2114–2120 (2014).
74. Liao, Y., Smyth, G. K. & Shi, W. featureCounts: an efficient general purpose program for assigning sequence reads to genomic features. *Bioinformatics* **30**, 923–930 (2014).

Acknowledgements The authors thank M. Long, W. Wang, L. Chen, W. Wang, X. Gao, P. Shi, Z. Shao, D. Wu, F. Xu, J. Zhang and L. Pu for their help. This work was supported by grants from the National Natural Science Foundation of China (32270438 and 32170498 to C.D., 32125005 and T2450075 to X.Z.), National Key R&D Program of China (2021YFF0702000 to C.D.), Noncommunicable Chronic Diseases–National Science and Technology Major Project (2023ZD0506800 to C.D.), 1.3.5 Project for Disciplines of Excellence, West China Hospital, Sichuan University (ZYCY21011 to C.D.), National Clinical Research Center for Geriatrics, West China Hospital, Sichuan University (Z2023JC003 to C.D.), Science and Technology Department of Sichuan Province (2022YFH0116 to C.D.), The CAS Project for Young Scientists in Basic Research (YSBR-097 to X.Z.).

Author contributions C.D. conceived and supervised the project. C.D., C.Z., X.X. and J.L. participated in research design. C.D., C.Z., X.X., J.L., Y.H., Q.S., S. Liu and S. Leng conducted experiments. C.D., C.Z., X.X., J.L., Q.S. and J.B. performed data analysis and interpretation. C.D. and C.Z. contributed Methods. J.L. contributed in vivo ADV injection and C.Z. contributed to mouse AAV injection experiments. J.L. contributed in vivo experiments of eggs and chicks. C.Z. and Y.H. contributed in vivo experiments of lizards, fish and birds. J.L. contributed to

Article

western blots. C.Z., X.X. and Y.H. contributed experiments of chicken breeding. C.Z. and J.L. contributed to receptor functional validation experiments. X.X. contributed promoter experiments. S. Liu and X.H. contributed to the phylogenetic analysis. Y.H. and P.H. contributed to the analysis of snRNA-seq data. Y.H. contributed to the analysis of RNA-sequencing data. J.X. contributed to the sequence alignment. C.D., C.Z., X.X., J.L., X.Z., Q.Q., S.Y. and J.B. wrote and revised the manuscript.

Competing interests The authors declare no competing interests.

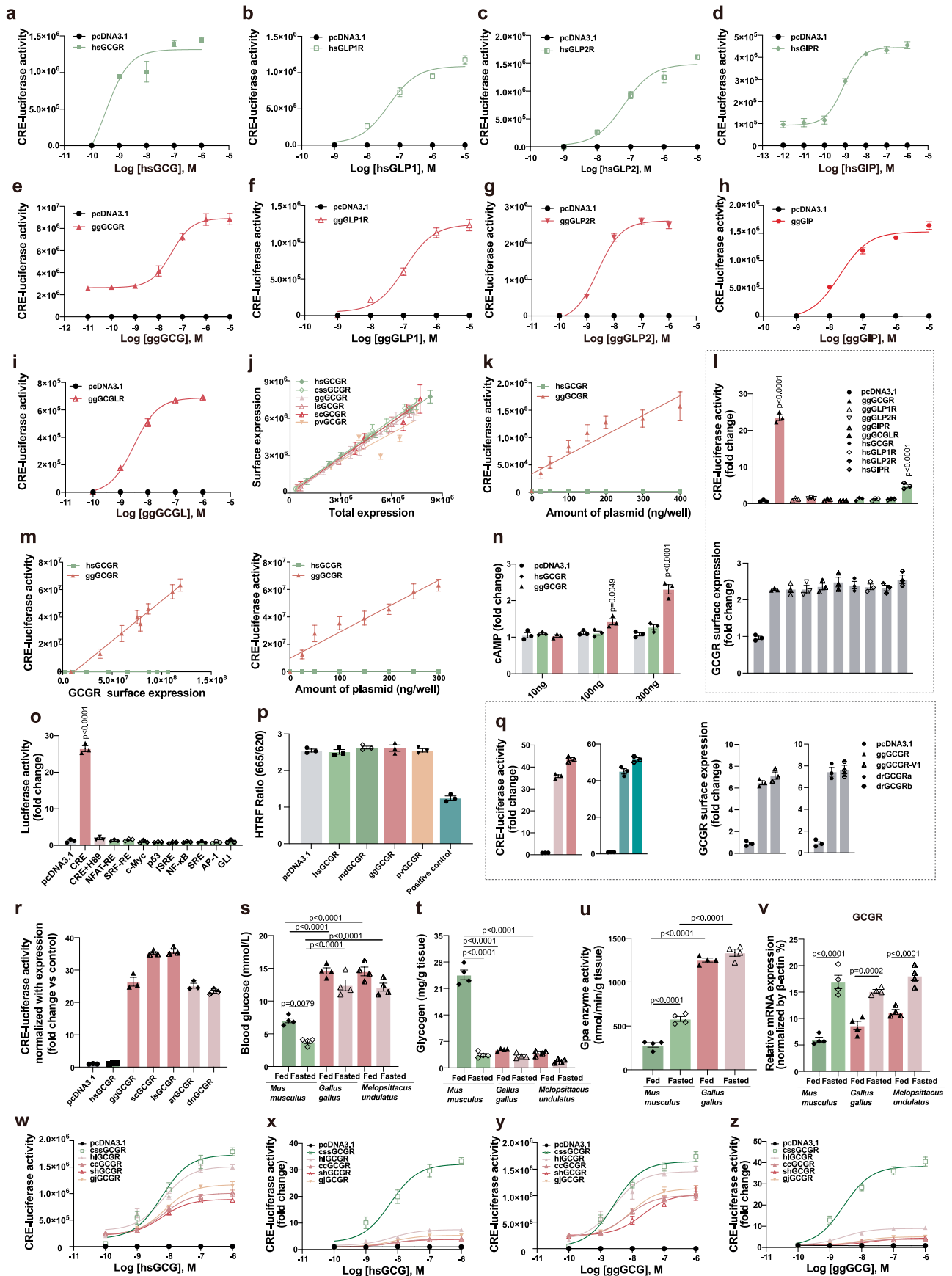
Additional information

Supplementary information The online version contains supplementary material available at <https://doi.org/10.1038/s41586-025-08811-8>.

Correspondence and requests for materials should be addressed to Cheng Deng.

Peer review information *Nature* thanks Ekaterina Osipova and the other, anonymous, reviewer(s) for their contribution to the peer review of this work. Peer review reports are available.

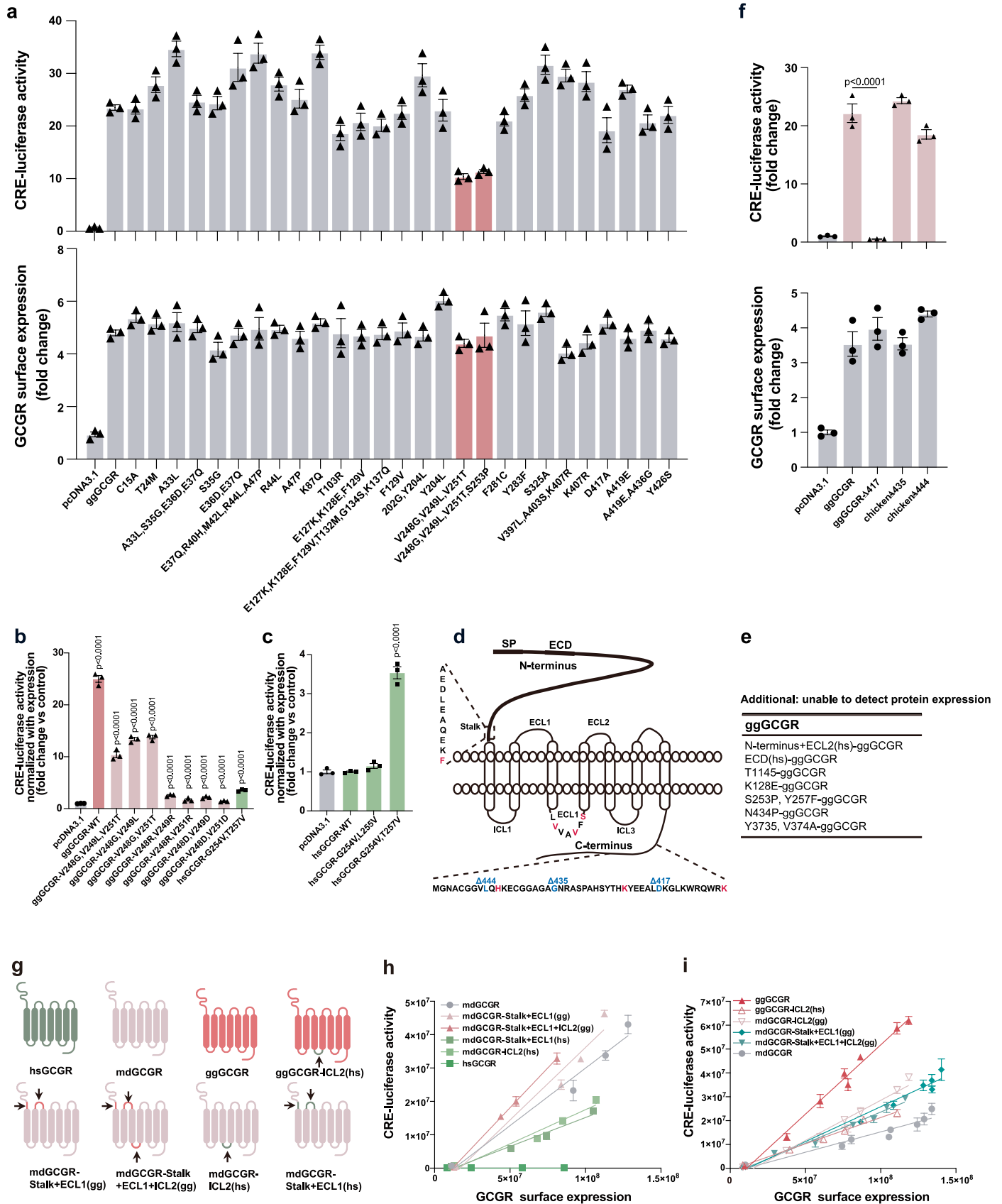
Reprints and permissions information is available at <http://www.nature.com/reprints>.



Extended Data Fig. 1 | See next page for caption.

Extended Data Fig. 1 | Functional tests of GCG receptor family. Related to Fig. 1. **a-i**, Concentration-response curves of GCG subfamily ligands to the *Homo sapiens* (hs) and *Gallus gallus* (gg) receptors in HEK293 cells. Due to differences in constitutive activity across the receptors, the y-axis scales in the Extended Data Fig. 1a-i are different. **j-m**, Constitutive activity in Gs signalling among the GCG receptor family. **n-p**, ggGCGR has constitutive activity in cAMP accumulation (**n**), not in other G protein signalling (**o**), especially IP1 accumulation (**p**). **q**, Two variants of ggGCGR and two homologous gene products of drGCGR have constitutive activity. **r**, Constitutive activities of GCGRs in different species, normalized by the expression of the plasmids. **s-v**, Changes in glucose metabolism and hepatic *GCGR* gene expression in different species under fed and fasting conditions. 16 h after starvation, blood glucose levels (**s**), glycogen content (**t**) and GPa enzyme activation (**u**) had been significantly

impacted in *Mus musculus*, but not in *Gallus gallus* and *Melopsittacus undulatus*. **v**, Fasting significantly increased the hepatic *GCGR* gene expression. n = 4/group. Primer sequences are shown in Supplementary Table 12. **w-z**, GCG stimulates the constitutively active GCGR. The activity of *Homo sapiens* (hs) GCG (**w**) and *Gallus gallus* (gg) GCG (**y**) stimulation of constitutively active GCGR (hlGCGR, ccGCGR, shGCGR, gjGCGR) was much lower than that of non-constitutively active GCGR (cssGCGR). **b,d**, Dose-response curves of hsGCG (**x**) and ggGCG to constitutively active GCGR (**z**). Abbreviations are listed in Supplementary Table 4. Peptide sequences are organized in Supplementary Table 13. Data are mean \pm SEM from at least three independent experiments, performed in technical triplicate. Data analysed by one-way ANOVA, Dunnett's post hoc test (**l,n,o**) and Tukey's post hoc test (**s-v**).

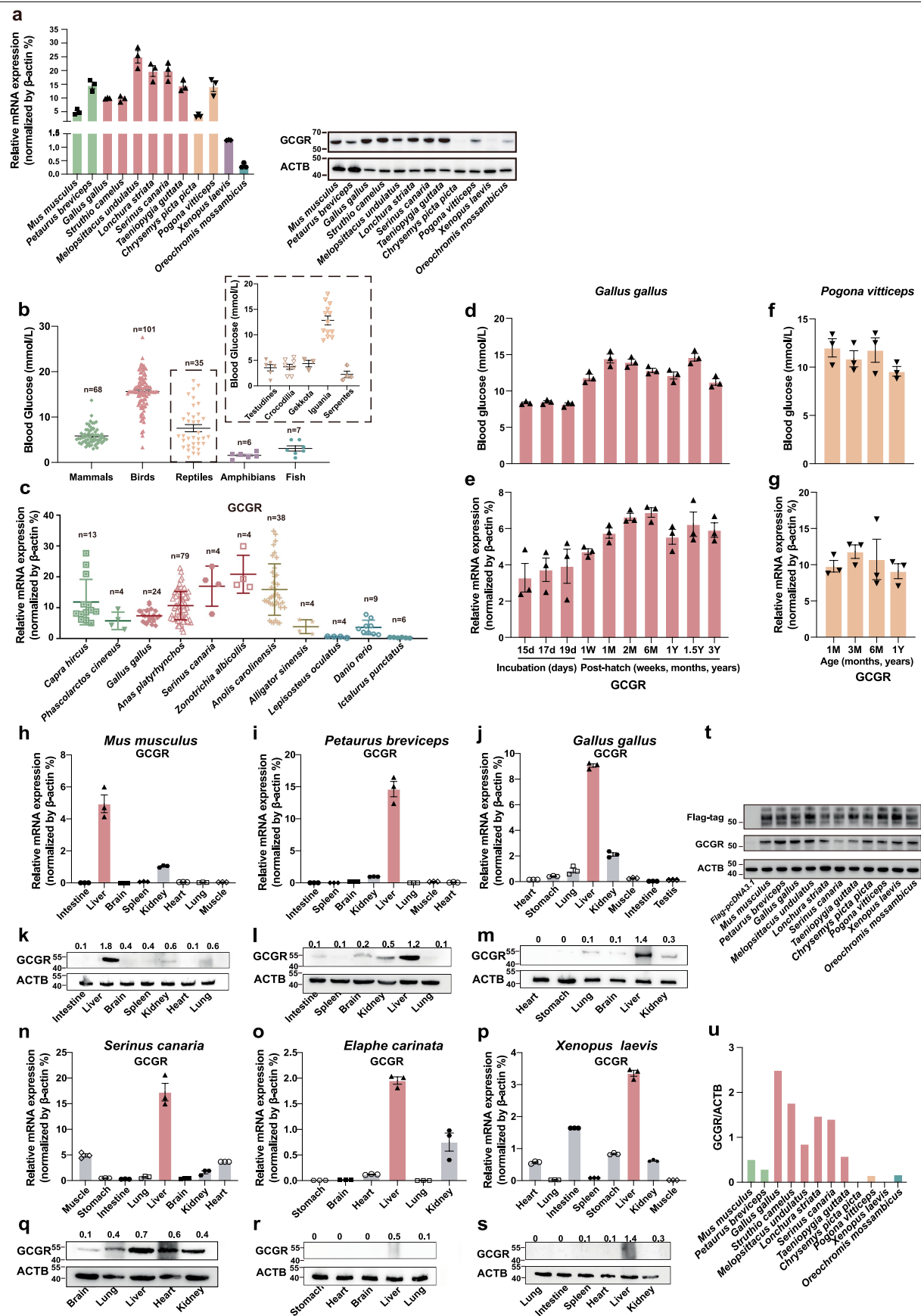


Extended Data Fig. 2 | See next page for caption.

Extended Data Fig. 2 | Functional tests of GCGR mutants. Related to Fig. 1.

a, Functional tests of those ggGCGR mutants (more conserved in birds and non-placental mammals as compared to placental mammals) well expressed in HEK293 cells. Expressed at a similar level, the ICL2 mutant (a triple mutant (Val248, Val249, Val251) and a quadruple mutant (Val248, Val249, Val251, Ser253) showed reduced constitutive activity compared with wild-type ggGCGR. The CDS sequences of the chicken *GCGR* gene that we used were derived from the GRCg7b/galGal1 genome assembly. Compared to the sequence of the wild form (red jungle fowl) (available as GRCg6a/galGal6), we only found three mismatches at the nucleotide level, all synonymous substitutions. **b,c**, Intracellular loop 2 (ICL2) mutations affected activity of ggGCGR and hsGCGR. **d**, Modified amino acids (highlighted in red) on the ggGCGR structure. Highlighted in blue represent the positions after which the

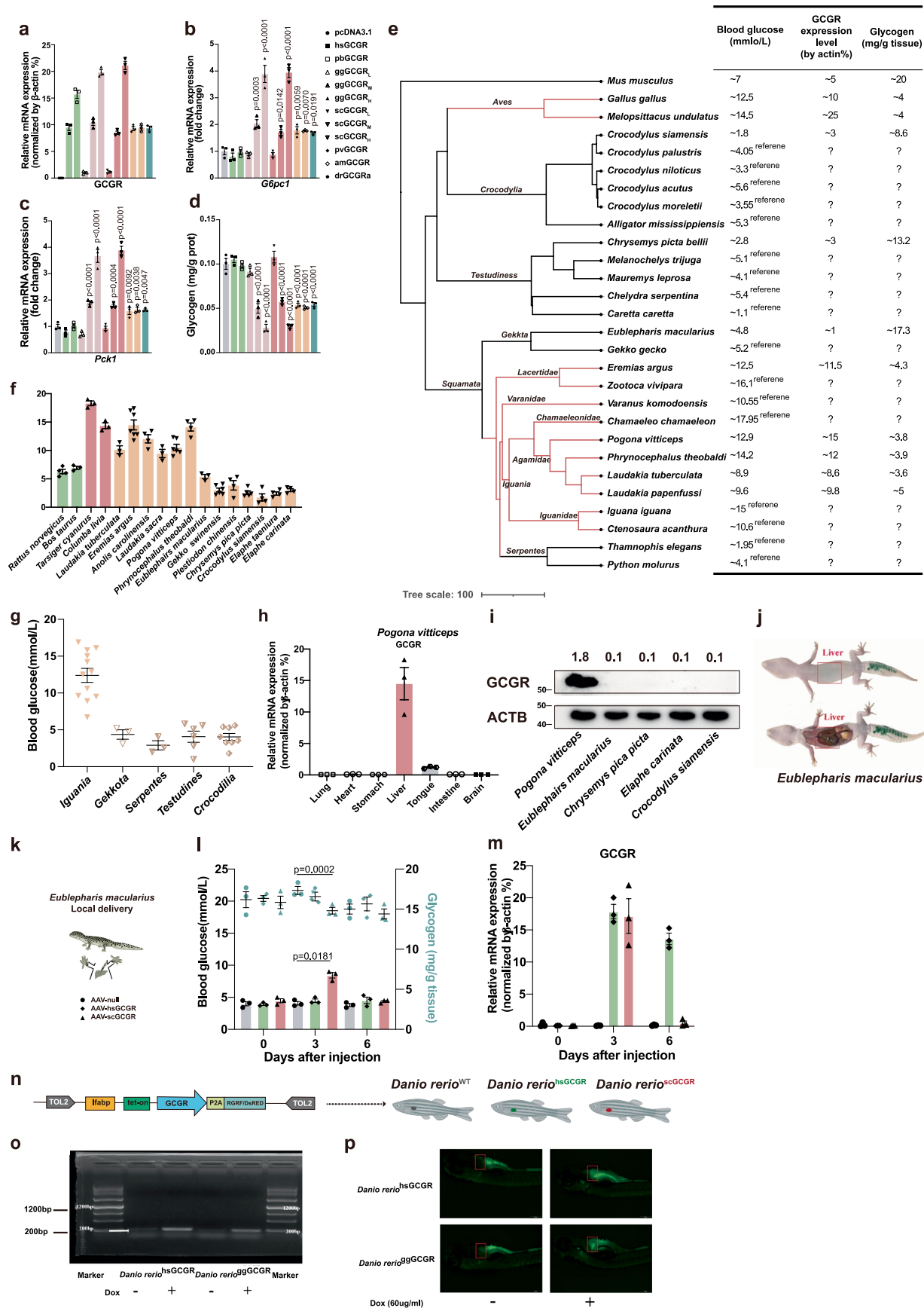
C-terminus was truncated. **e**, List of mutations that impaired receptor expression. **f**, C-terminal truncations decreased the constitutive activity of ggGCGR in HEK293 cells. Data are mean \pm SEM from at least three independent experiments, performed in technical triplicate. **g**, Schematic and functional verification of the different GCGR domain swaps. mdGCGR (opossum, a non-placental mammal with weak constitutive activity) mutated toward bird ggGCGR (**h**) or placental mammalian hsGCGR (**i**). After domain swapping with ggGCGR, the potency of constitutive activity in mdGCGR increased, while swapping with hsGCGR, the constitutive activity decreased. Statistically significant differences between GCGRs and pcDNA3.1 were analysed by one-way ANOVA and Dunnett's post hoc test (**b,c**). Data are mean \pm SEM from at least three independent experiments, performed in technical triplicate. Cartoons were created with BioRender.com.



Extended Data Fig. 3 | See next page for caption.

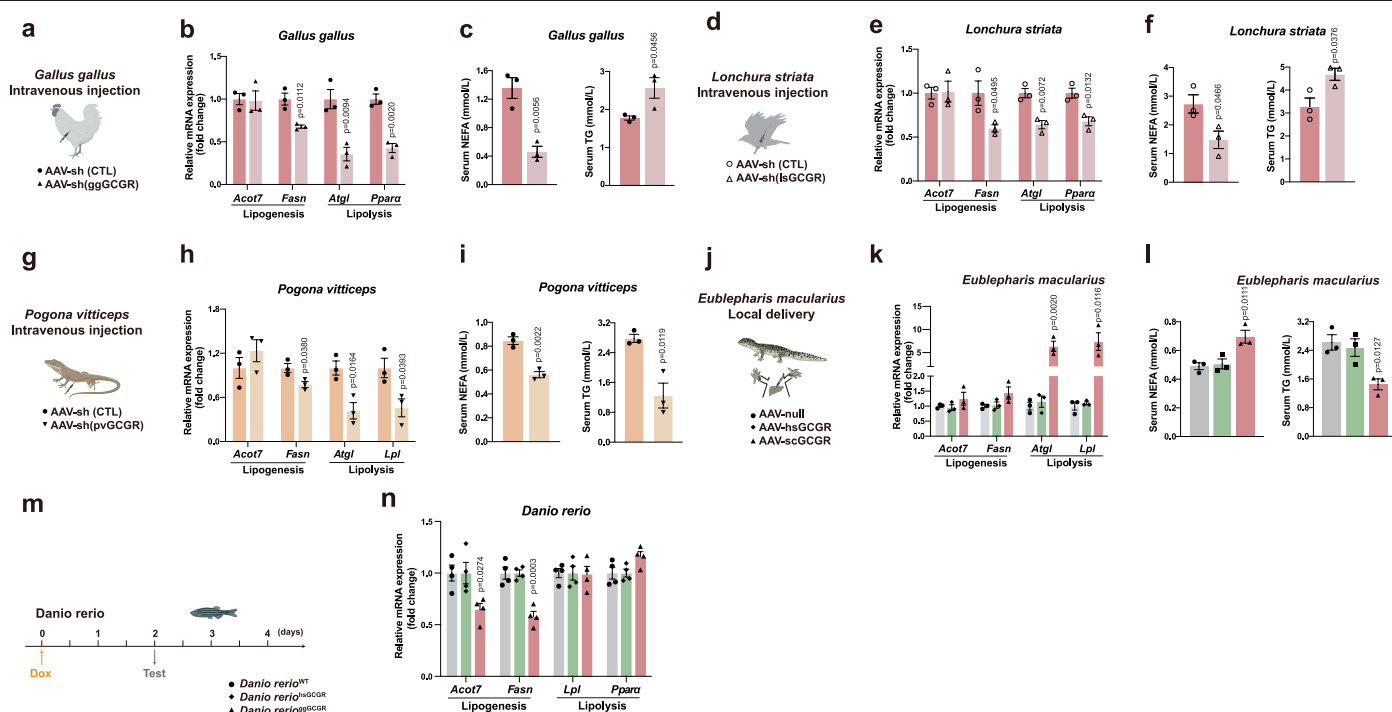
Extended Data Fig. 3 | High blood glucose sustained by high hepatic *GCGR* gene expression. Related to Fig. 1. a, mRNA and protein expression in the livers of different species. **b**, Birds and *Iguania* have high blood glucose levels among vertebrates. Blood glucose levels are taken from references organized in Supplementary Table 1. n: number of species. **c**, Birds and *Iguania* sustained high hepatic *GCGR* expression in vertebrates. Hepatic *GCGR* gene expression levels were derived from RNA-sequencing data. References are organized in Supplementary Table 7. Data represent mean \pm SEM. n: individuals. **d-g**, Blood glucose levels and *GCGR* mRNA expression during the whole life in *Gallus gallus* (day 1 is defined as the first day of egg incubation) and *Pogona vitticeps* at various ages. During the whole life, blood glucose and hepatic *GCGR* gene expression increased continuously and high levels were sustained in *Gallus gallus* (**d,e**), as well as in *Pogona vitticeps* (**f,g**). n = 3/group. Data represent mean \pm SEM. **h-u**, RT-qPCR and Western blot detection of *GCGR* expression in

tissues from different species. *GCGR* gene is highly expressed in liver; birds and non-placental mammals have the highest expression levels in various species, whether at mRNA (**h-j,n-p**) or protein levels (**k-m,q-s**). Data represent mean \pm SEM. n = 3/group. **t**, *GCGR* constructs from different species with an N-terminal Flag tag were cloned into pcDNA3.1 (fusion expression) and transiently transfected into HEK293T cells. Western blot analysis was performed using anti-FLAG and anti-*GCGR* antibodies to detect protein expression levels, and band intensity comparison was used to validate the antibody efficacy. **u**, Band intensities. The intensities of immunoreactivity bands was measured using NIH image software, ImageJ, and all bands were normalized to percentages of ACTB control values. Statistics are shown above the Western blot analysis of each tissue. All software and instruments used are organized in Supplementary Table 16. Data are mean \pm SEM from at least three independent experiments, performed in technical triplicate.



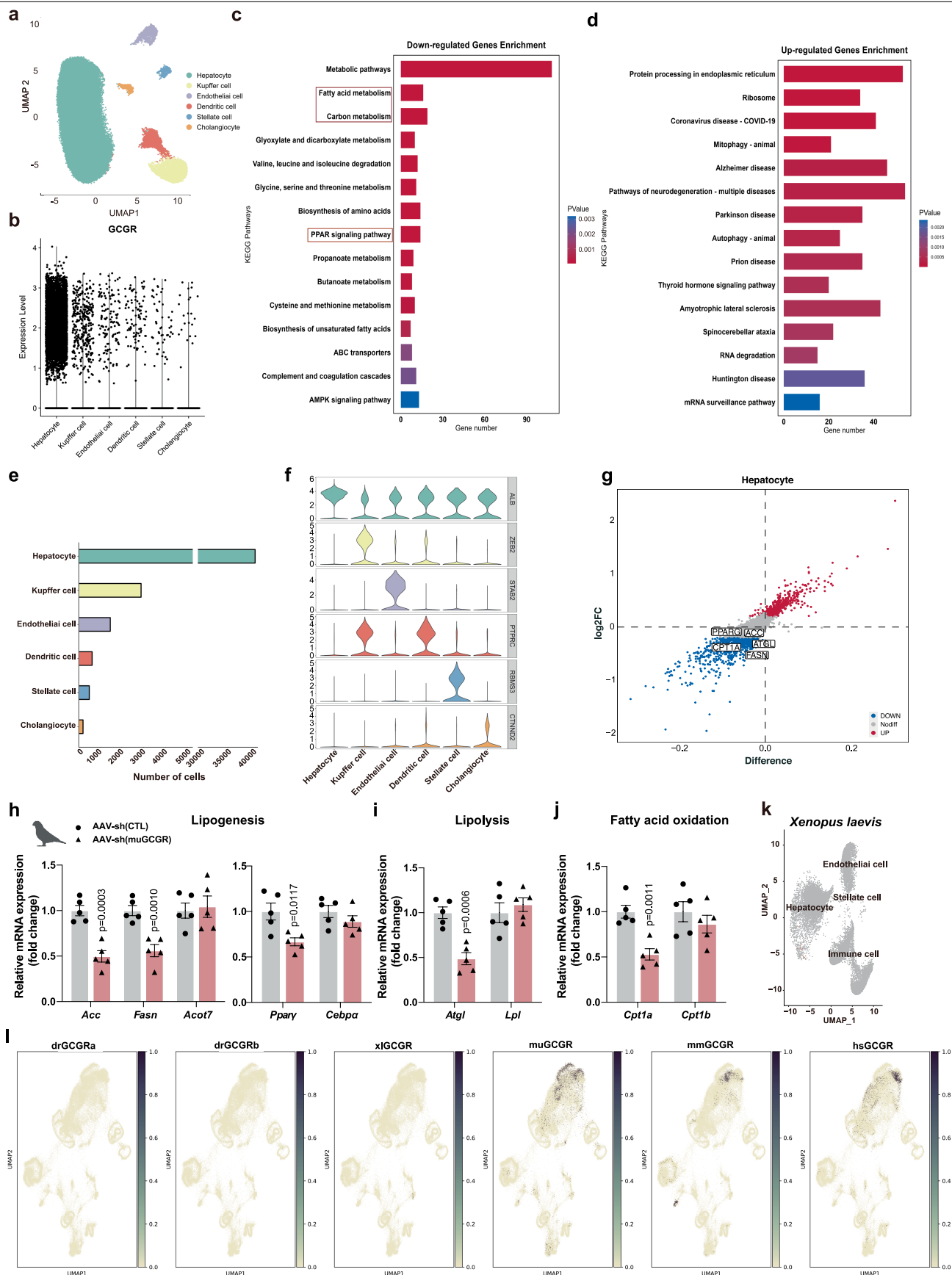
Extended Data Fig. 4 | The hepatic GCGR level determines the blood glucose level in reptiles and fishes. Related to Fig. 2. **a**, mRNA levels of *hsGCGR*, *Petaurus breviceps* (pb) GCGR, *ggGCGR_L*, *ggGCGR_M*, *ggGCGR_H*, *scGCGR_L*, *scGCGR_M*, *scGCGR_H*, *pvGCGR*, *Alligator mississippiensis* (am) GCGR, and *Danio rerio* (dr) GCGRa genes in AML12. **b-d**, The effect of GCGR overexpression from different species on intracellular *G6pc1* (**b**), *Pck1* (**c**), and intracellular glycogen content (**d**). *n* = 3/group. **e-g**, Phylogenetic tree of reptile species (**e**), hepatic *GCGR* gene expression (**f**) and blood glucose levels (**g**) in reptiles based on our data and references organized in Supplementary Table 1. **h**, Among various tissues, *GCGR* gene expression is the highest in the liver of *Pogona vitticeps*. *n* = 3/group. Data are presented as the mean \pm SEM. **i**, Hepatic *GCGR* gene expression in *Pogona vitticeps* is relatively high among reptiles. The density of immunoreactive bands were measured using NIH image software, ImageJ, and all bands were normalized to percentages of β -actin control values. Statistics are shown above the western blot analysis of each tissue. **j**, Schematic of AAV in situ liver injection in *Eublepharis macularius*. **k-m**, constitutively active GCGR expression in liver results in high blood glucose in *Eublepharis macularius*.

k, Schematic of the AAV local delivery used to overexpress *hsGCGR* or *scGCGR* in the liver of *Eublepharis macularius*. Created in BioRender; Quanwei, Y. (2025), <https://BioRender.com/c76s860>. **l,m**, The blood glucose levels, liver glycogen content (**l**) and hepatic *GCGR* gene mRNA expression (**m**) was affected by AAV-*scGCGR* and AAV-*scGCGR* (approximately 16% and 15% of β -actin, respectively) in liver after 3-day injection. *n* = 3/group. **n-p**, Construction and identification of conditional knock-in zebrafish, *Danio rerio*. Strategy of conditional knock-in *Danio rerio*. *lfabp* (liver fatty acid binding protein): the promoter of liver-specific fatty acid binding protein in *Danio rerio* (**n**; created in BioRender; Quanwei, Y. (2025), <https://BioRender.com/jl1v652>). Identification of doxycycline (Dox) induced GCGR DNA (**o**) and protein expression levels (**p**) in conditional knock-in adult *Danio rerio*. Three days after Dox induction *GCGR* gene expression was monitored. The red box indicates the area of hepatic *hsGCGR* and *ggGCGR* gene overexpression in *Danio rerio*^{*hsGCGR*} and *Danio rerio*^{*ggGCGR*}, respectively. Data are mean \pm SEM from at least three independent experiments, performed in technical triplicate, and analysed by one-way ANOVA and Dunnett's post hoc test (**a-d,l**). The *p* values are displayed for the comparison with pcDNA3.1 group (**a-d**).



Extended Data Fig. 5 | Constitutively active hepatic GCGR expression positively regulates downstream the lipid metabolism pathway. Related to Fig. 2. a,d,g,j,m. Schematic of AAV-sh(ggGCGR) *i.v.* injection in *Gallus gallus* (chicks) (n = 3/group) (a), *Lonchura striata* (n = 3/group) (d), *Pogona vitticeps* (n = 3/group) (g), *Eublepharis macularius* (n = 3/group) (j), *Danio rerio* (n = 4/group) (m). **b,e,h,k,n.** Hepatic lipogenesis gene (*Acot7* and *Fasn*) and lipolysis gene (*Atgl*, *Ppara* or *Lpl*) expression (mRNA) 10 days after AAV-sh(ggGCGR) *i.v.* injection in chicks (b), 4 days after AAV-sh(lgGCGR) *i.v.* injection in *Lonchura striata* (e), 5 days after AAV-sh(pvGCGR) *i.v.* injection in *Pogona vitticeps* (h), three days after AAV-scGCGR *i.v.* injection in *Eublepharis macularius* (k) and

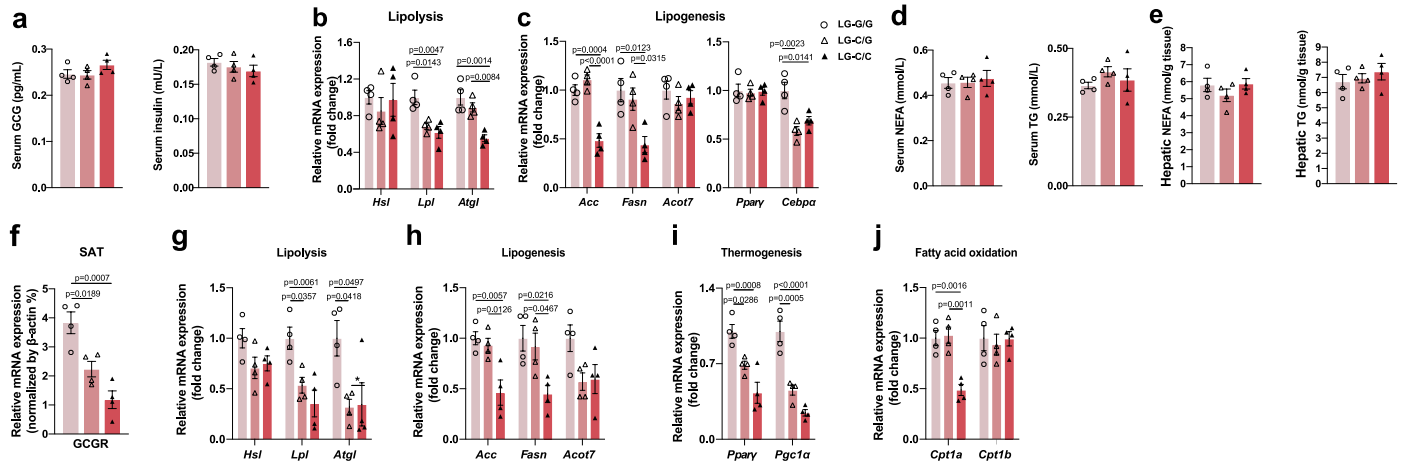
24 h after DOX induction in *Danio rerio* (n). **c,f,i,l.** Serum NEFAs and TGs content 10 days after AAV-sh(ggGCGR) *i.v.* injection in chicks (c), 4 days after AAV-sh(lgGCGR) *i.v.* injection in *Lonchura striata* (f), 5 days after AAV-sh(pvGCGR) *i.v.* injection in *Pogona vitticeps* (i), three days after AAV-scGCGR *i.v.* injection in *Eublepharis macularius* (l). Data are mean \pm SEM from at least three independent experiments, performed in technical triplicate, and analysed two-tailed unpaired Student's *t* test (b,c,e,f,h,i) and analysed by one-way ANOVA and Dunnett's post hoc test (k,l,n). Cartoons were created in BioRender; Quanwei, Y. (2025), <https://BioRender.com/j11v652>.



Extended Data Fig. 6 | See next page for caption.

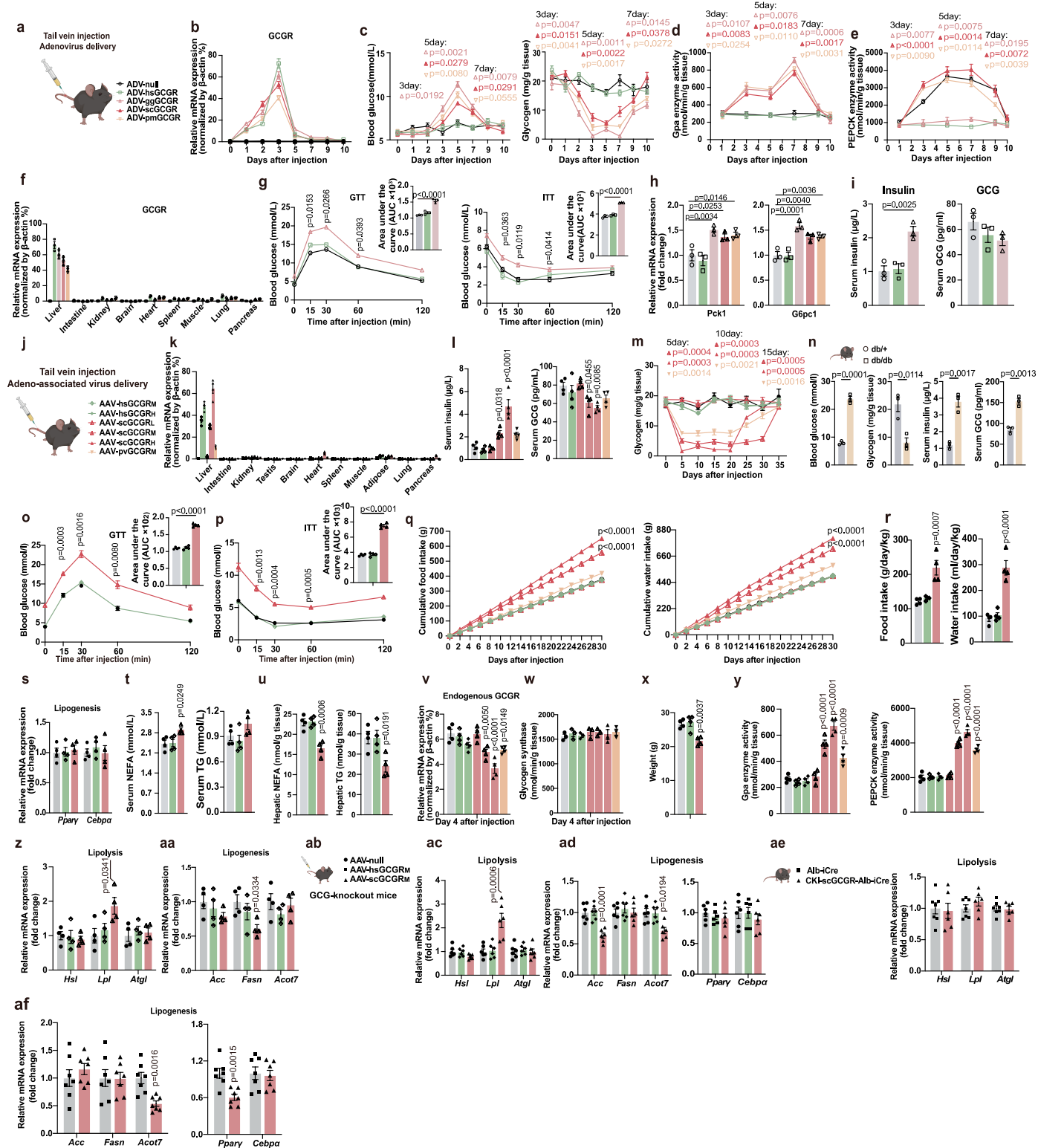
Extended Data Fig. 6 | Avian constitutively active GCGR regulates downstream the lipid metabolism pathway. Related to Fig. 3. a-c, sNuc-RNAseq of liver three days after injection. UMAP (n = 3) (a). Violin plots (b). KEGG pathways enriched for down-regulated genes (c) and up-regulated genes (d). **e-g,** Integration of sequenced budgerigar cells in liver and stratification into six different cell types (N = 3 individuals, n = 45666 cells) (e), marker genes for each cell type in the budgerigar (f), differential gene expression (g) analysis using the log2-fold change expression and the difference in the percentage of cells expressing the gene comparing the AAV-null and AAV-shGCGR budgerigar hepatocyte groups. **h-j,** Lipogenesis genes (*Acc*, *Fasn* and *Acot7*, *Pparγ*, *Cebpa*)

(**h**; created in BioRender; Quanwei, Y. (2025), <https://BioRender.com/j11v652>), lipolysis genes (*Atgl* and *Lpl*) (**i**), and fatty acid oxidation genes mRNA expression three days after injection (**j**). n = 3/group. **k,** Map plot colour-coded for expression (gray to red) of *GCGR* gene across the liver of *Xenopus laevis*. **l,** Map plot colour-coded for expression of *GCGR* gene across the liver of *Danio rerio* (dr), *Xenopus laevis* (xl), *Mus musculus* (mm), *Melopsittacus undulatus* (mu), *Homo sapiens* (hs). Data are mean ± SEM from at least three independent experiments, performed in technical triplicate, and analysed two-tailed unpaired Student's *t* test.



Extended Data Fig. 7 | An eSNP in the promoter of the *GCGR* gene was identified after selection of chickens (outbred) for high or low blood glucose. Related to Fig. 3. a, Serum GCG and insulin levels detected in 60-day-old male C/C and its littermates C/G and G/G of F3 generation. $n = 4$ /group. **b,c**, Lipolysis genes (*Hsl*, *Lpl* and *Atgl*) (**b**), lipogenesis genes (*Acc*, *Acot7*, *Fasn*, *Pparγ* and *Cebpa*) expression (mRNA) (**c**) detected in 60-day-old male C/C and littermates C/G and G/G of F3 generation. $n = 4$ /group. **d,e**, Serum (**d**) and hepatic NEFAs, and TGs (**e**), were detected in 60-day-old male C/C and

littermates C/G and G/G of F3 generation. $n = 4$ /group. **f-j**, *GCGR* gene (**f**), lipolysis genes (*Hsl*, *Atgl*, *Lpl*) (**g**), lipogenesis genes (*Acc*, *Acot7*, *Fasn*) (**h**) and thermogenesis genes (*Pparγ*, *Pgc1α*) (**i**), fatty acid oxidation genes (*Cpt1a*, *Cpt1b*) (**j**) expression levels in subcutaneous adipose tissue (SAT) of 60-day-old male C/C and its littermates C/G and G/G. Data are mean \pm SEM from at least three independent experiments, performed in technical triplicate, and analysed by one-way ANOVA and Tukey's post hoc test (**a-j**).

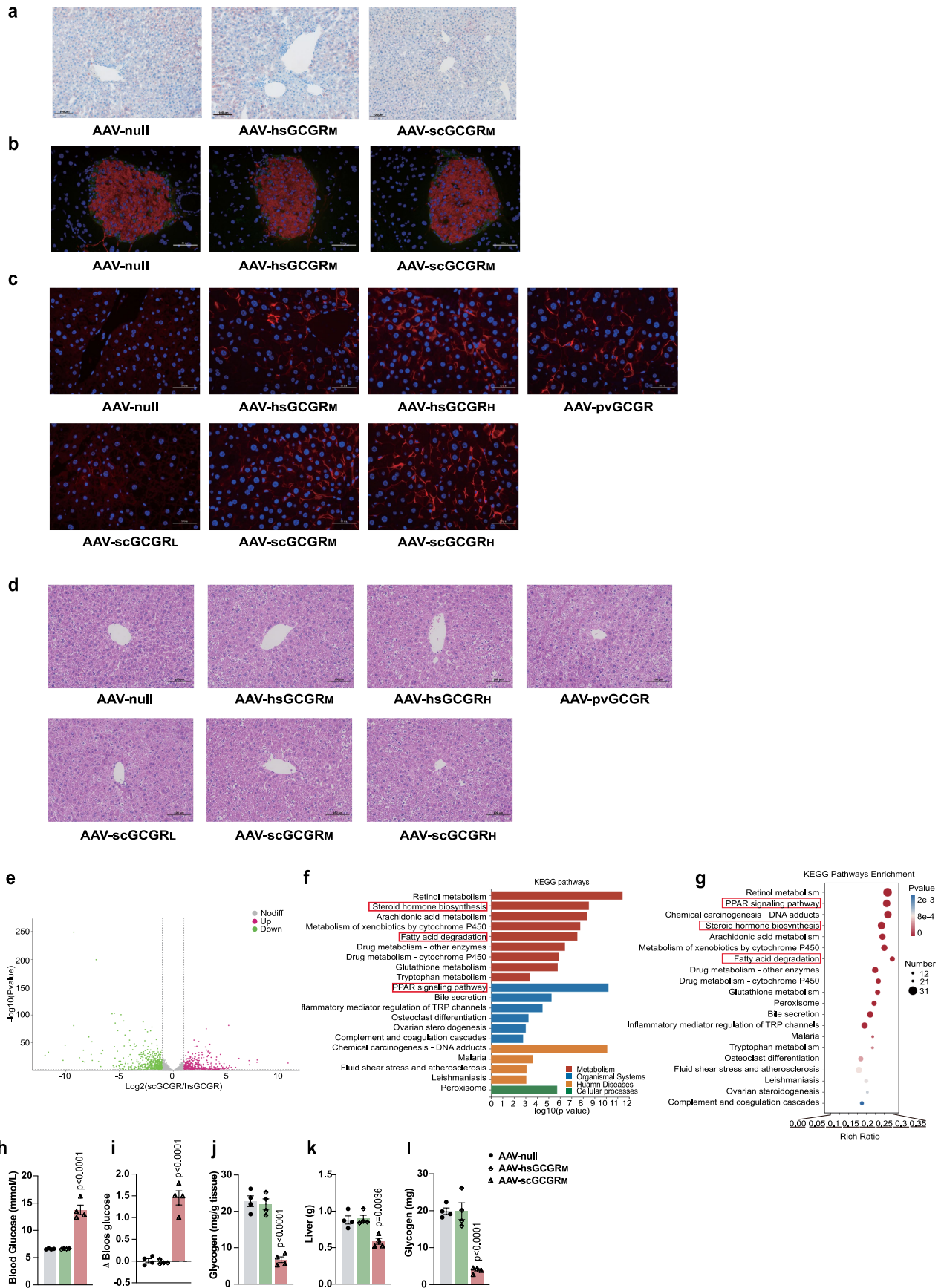


Extended Data Fig. 8 | See next page for caption.

Article

Extended Data Fig. 8 | Constitutively active GCGR, expressed at avian hepatic levels by ADV and AAV injection, results in sustained high blood glucose in mice. Related to Fig. 4. a-c, Schematic depicting tail vein adenovirus (ADV) injections (**a**). Transient hepatic overexpression of hsGCGR (ADV-hsGCGR), ggGCGR (ADV-ggGCGR), scGCGR (ADV-scGCGR), and a snake *Protophthalmos mucrosquamatus*, (pm) GCGR (ADV-pmGCGR) in the liver. hsGCGR, ggGCGR, scGCGR, and pmGCGR mRNA levels (**b**), blood glucose levels and glycogen content (**c**) were made within 10 days after injection. n = 3/group. **d,e**, GPa and PEPCK enzyme activity were detected at different time points within 10 days after injection. n = 3/group. **f**, The various ADV-GCGR constructs were delivered to the liver for high-level expression three days after injection. n = 3/group. **g**, Glucose tolerance test (GTT) and insulin tolerance test (ITT) in null-, hsGCGR-, and ggGCGR-injected mice four days after injection. n = 3/group. **h**, The effect of hsGCGR, ggGCGR, ccGCGR, and pmGCGR overexpression (5 days after injection) on *Pck1* and *G6pc1* mRNA expression. n = 3/group. **i**, Constitutively active GCGR enhanced serum insulin concentration, but not glucagon five days after injection. n = 3/group. **j**, Schematic of the tail vein and adeno-associated virus (AAV) injections (cartoons created with BioRender.com). Continuous hepatic overexpression of hsGCGR (AAV-hsGCGR), scGCGR (AAV-scGCGR), and pvGCGR (AAV-pvGCGR) in the liver. **k**, The constructed AAV vector specifically delivered GCGR to the liver for high expression seven days after injection. n = 4/group. **l**, Constitutively active GCGR-injected mice showed increased serum insulin concentrations and decreased glucagon concentrations 4 days after injection. n = 4/group. **m**, Measurements of glycogen content were made within 35 days. n = 4/group. **n**, *db/db* mice had increased blood glucose levels, serum insulin and glucagon concentration, while liver glycogen content decreased compared to the

control mice (*db/+*) 15 days after injection. n = 3/group. **o,p**, GTT and ITT tests in AAV-null, AAV-hsGCGR_M, and AAV-scGCGR_M mice 10 days after injection. n = 4/group. **q,r**, constitutively active GCGR-injected mice showed increased cumulative food and water intake within 30 days after injection. **s**, Hepatic lipogenesis gene expression (*Ppar γ* and *Cebpa*) 15 days after injection. n = 4/group. **t,u**, Serum NEFAs (non-esterified fatty acids) (**t**), TGs (triglycerides), and hepatic NEFAs, TGs, content (**u**) 15 days after AAV-null, AAV-hsGCGR_M and AAV-scGCGR_M *i.v.* injection in mice. n = 4/group. **v**, Endogenous *GCGR* gene expression in each group. n = 4/group. **w**, AAV injection did not affect the activity of endogenous glycogen synthase. n = 3/group. **x**, AAV-scGCGR_H mice showed decreased body weight 25 days after injection. n = 4/group. **y-aa**, GPa, PEPCK enzyme activity (**y**), *Hsl*, *Lpl*, *Atgl* (**z**), *Acc*, *Acot7*, *Fasn* (**aa**) levels. High (H), medium (M), low (L) represent different AAV titres (details in Methods). **ab-ad**, Schematic of the tail vein and adeno-associated virus (AAV) injections (**ab**). Hepatic lipolysis genes (*Hsl*, *Lpl*, *Atgl*) (**ac**) and lipogenesis genes (*Acc*, *Acot7*, *Fasn*) (**ad**) expression (mRNA) 15 days after AAV-hsGCGR and scGCGR *i.v.* injection in GCG-knockout mice. n = 6/group. **ae**, Hepatic lipolysis genes (*Hsl*, *Lpl* and *Atgl*) mRNA expression 15 days after Dox induction in CKI mice. n = 7/group. Data are presented as the mean \pm SEM and analysed by two-way ANOVA followed by Dunnett's post hoc test (**c-e**, **g,m,o-q**), one-way ANOVA and Dunnett's post hoc test (**h,i,l,r-ad**), two-tailed unpaired Student's t test (**n,ae,af**). The *p* values are displayed for the comparison with control group (ADV-null or AAV-null). H: high exogenous expression of GCGR (5×10^{11} vg per mouse); M: medium exogenous expression of GCGR (1×10^{11} vg per mouse); L: low exogenous expression of GCGR (1×10^{10} vg per mouse). Cartoons were created in BioRender; Quanwei, Y. (2025), <https://BioRender.com/i08h417>.



Extended Data Fig. 9 | See next page for caption.

Extended Data Fig. 9 | Immunofluorescence, haematoxylin-eosin staining (H&E staining) images and RNA-seq data from AAV injected mice. Related to Fig. 4. **a**, Oil red staining of AAV- null-, AAV-hsGCGR_M- and AAV-scGCGR_M- injected mice. **b**, No pathology effect on mouse pancreas seven days after injection from immunofluorescence images. Blue represents DAPI, green represents α -cells and red represents β -cells. The quantified results are located on the right. **c,d**, According to the immunofluorescence image observed on day seven (**c**) and he haematoxylin-eosin staining (H&E staining) (**d**) obtained on day 15, there were no pathological changes in the liver of mice after AAV

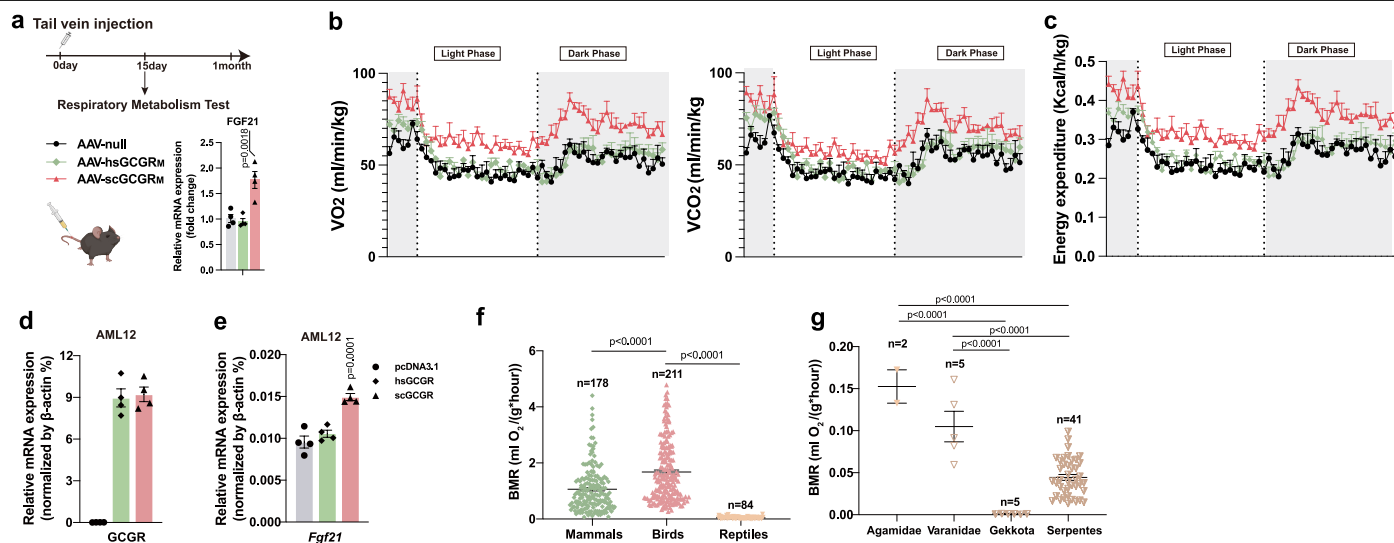
injection. Blue represents DAPI and red represents V5. Scale bar, 100 μ m. **e**, Patterns of differentially expressed genes (DEGs) between scGCGR_M and null groups. **f**, Functional pathways enrichment of differential genes between scGCGR_M and hsGCGR_M groups. **g**, Top 12 KEGG pathways enrichment of upregulated genes in liver of AAV-injected mice. **h**, 25 days after AAV injection, change of blood glucose in AAV with hsGCGR_M- and scGCGR_M-mice and its contribution to weight loss (**i**). **j-l**, The constitutively active GCGR-injected mice showed decreased glycogen content (**j**), liver weight (**k**) and its contribution to body weight (**l**) 25 days after injection. n = 4/group.



Extended Data Fig. 10 | Overexpressing GCGR with modest constitutive activity in mouse liver results in a similar but more modest phenotype in comparison to the constitutively active GCGR group. Related to Fig. 4.

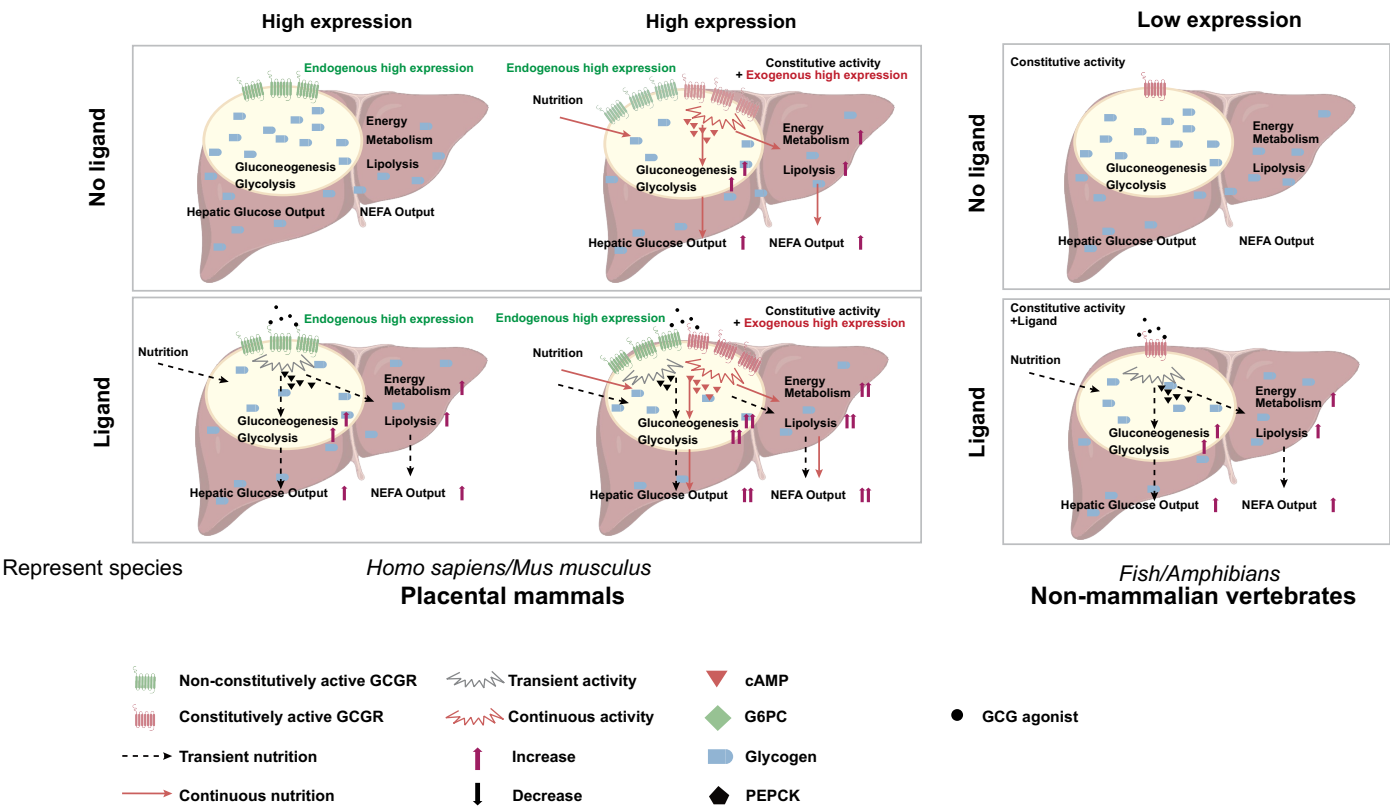
a, Schematic of the tail vein and AAV injection to overexpress hsGCGR, hsGCGR^{H339R}_H or pbGCGR_H (H: high dose) in the liver of mice. Both hsGCGR^{H339R} and pbGCGR had weak constitutive activity (detected in HEK293 cells). **b**, Measurements of blood glucose and body weight within 28 days after injection. n = 4/group. **c**, Hepatic overexpression of hsGCGR (approximately 150% of β -actin) in the liver 15 days after injection. n = 4/group. **d**, Gluconeogenesis genes (*G6pc1* and *Pck1*) mRNA expression 15 days after injection in mice. n = 4/group. **e,f**, Glycogen content (**e**), and GPα enzyme activity (**f**) in the liver were detected after 15 days of AAV injection. n = 4/group. **g,h**, Lipolysis genes (*Hsl*, *Lpl*, and *Atgl*) (**g**), lipogenesis genes (*Acc*, *Acot7*, *Fasn*, *Pparγ*, and *Cebpa*) expression (**h**) (mRNA) 15 days after injection in mice. n = 4/group. **i,j**, Serum NEFAs (**i**) and TGs and hepatic NEFAs (**j**) and TGs content 15 days after injection in mice. n = 4/group. **k**, Transient hepatic pbGCGR expression of AAV-pbGCGR-injected mice within 14 days (approximately 60% of β -actin) in liver, and the mRNA levels of hepatic glycogenolysis genes (*G6pc1* and *Pck1*) at day four after injection. n = 4/group. **l-n**, Hepatic glycogenolysis genes (*G6pc1* and *Pck1*) (**l**), lipolysis genes (*Atgl*, *Hsl* and *Lpl*) (**m**) and lipogenesis genes (*Acc*, *Acot7*, *Fasn*, *Pparγ* and *Cebpa*) (**n**) expression (mRNA) 15 days after pbGCGR i.v. injection in mice. n = 4/group. **o,p**, Serum (**o**) and hepatic NEFAs and TGs content (**p**) 15 days

after pbGCGR i.v. injection in mice. n = 4/group. **q**, Schematic of adeno-associated virus delivery (AAV) injections of hsGCGR and scGCGR into the tail vein of C57BL/6 J male mice (after 23-week HFD feeding). n = 6/group. **r**, Measurements of blood glucose and body weight within 24 days after AAV injection, respectively. **s**, mRNA levels of scGCGR_H and hsGCGR_H gene expression in liver 18 days after injection. **t**, Hepatic glycogenolysis genes (*G6pc1* and *Pck1*), **u**, lipolysis genes (*Hsl*, *Lpl* and *Atgl*), **v**, lipogenesis genes (*Acc*, *Acot7*, *Fasn*, *Pparγ* and *Cebpa*) expression (mRNA) 20 days after AAV-hsGCGR and scGCGR i.v. injection in HFD mice. **w-z**, RNA-sequencing data of liver five (left) and 18 (right) days after scGCGR_H i.v. injection in HFD mice. RNA-sequencing data showing changes in glycogenolysis genes (*G6pc* and *Pck1*) (**w**) following GCGR overexpression in mice 5 days after injection, and lipolysis gene (*Lpl*) and lipogenesis genes (*Pparγ*, *Fasn*) following GCGR overexpression in mice 18 days after injection. Patterns of differentially expressed genes (DEGs) between scGCGR_H and hsGCGR_H (**x**). The top 20 significantly enriched KEGG pathways of differently expressed genes of liver in mice 18 days after injection (**y,z**). Data are presented as the mean \pm SEM and analysed by two-way ANOVA followed by Dunnett's post hoc test (**b,r**), one-way ANOVA and Dunnett's post hoc test (**a,c,j,t-v**), two-tailed unpaired Student's *t* test (**k-p,s**). The *p* values are displayed for the comparison with control group (AAV-null). Cartoons were created in BioRender; Quanwei, Y. (2025), <https://BioRender.com/i08h417>.



Extended Data Fig. 11 | Constitutively active GCGR expression in the liver increases the basal metabolism rate. Related to Fig. 4. **a**, Schematic depicting tail vein AAV injection and the hepatic *Fgf21* mRNA expression in null-, hsGCGR_M- and scGCGR_M-injected mice 15 days after injection (cartoons created with BioRender.com). *n* = 4/group. Created in BioRender; Quanwei, Y. (2025), <https://BioRender.com/i08h417>. **b,c**, VO₂ consumption and VCO₂ consumption (**b**), and energy consumption (**c**) by indirect calorimetry in null-, hsGCGR_M- and scGCGR_M-injected mice 15 days after the AAV injection. *n* = 5/group.

d,e, Overexpression of constitutively active GCGR in AML12 cells upregulated energy metabolism-related fibroblast growth factor gene- *Fgf21*. **f**, Birds show higher basal metabolic rates than mammals and reptiles. *n*: number of species. **g**, *Agamidae* and *Varanidae* show higher basal metabolic rates among reptiles. *n*: individuals. References are organized in Supplementary Table 11. Data are presented as the mean ± SEM and analysed by one-way ANOVA, Dunnett's post hoc test (**a,d,e**), and Tukey's post hoc test (**f,g**). Cartoons were created with BioRender.com.



Extended Data Fig. 12 | Model of mechanisms regulating the glycemic effects of GCGR. Related to Fig. 5. Owing to the low hepatic levels, constitutively active GCGRs in non-mammalian vertebrates (fish and amphibians) up-regulated glycogenolysis, gluconeogenesis, lipolysis energy metabolism through GCG agonist stimulation. Left: in livers of placental mammals, GCGRs devoid of constitutive activity are highly expressed. Gs signalling and subsequent upregulation of glucose and lipid metabolism only occur upon ligand stimulation. Middle: heterologous overexpression of constitutively active GCGR in mouse liver activates Gs signalling and upregulates glucose and lipid metabolism, even without ligand stimulation. Right: constitutively active GCGR is modestly expressed in the liver, activating Gs signalling and upregulating glucose and lipid metabolism only upon ligand binding.

Reporting Summary

Nature Portfolio wishes to improve the reproducibility of the work that we publish. This form provides structure for consistency and transparency in reporting. For further information on Nature Portfolio policies, see our [Editorial Policies](#) and the [Editorial Policy Checklist](#).

Statistics

For all statistical analyses, confirm that the following items are present in the figure legend, table legend, main text, or Methods section.

- | | |
|-------------------------------------|--|
| n/a | Confirmed |
| <input type="checkbox"/> | <input checked="" type="checkbox"/> The exact sample size (<i>n</i>) for each experimental group/condition, given as a discrete number and unit of measurement |
| <input type="checkbox"/> | <input checked="" type="checkbox"/> A statement on whether measurements were taken from distinct samples or whether the same sample was measured repeatedly |
| <input type="checkbox"/> | <input checked="" type="checkbox"/> The statistical test(s) used AND whether they are one- or two-sided
<i>Only common tests should be described solely by name; describe more complex techniques in the Methods section.</i> |
| <input type="checkbox"/> | <input checked="" type="checkbox"/> A description of all covariates tested |
| <input type="checkbox"/> | <input checked="" type="checkbox"/> A description of any assumptions or corrections, such as tests of normality and adjustment for multiple comparisons |
| <input type="checkbox"/> | <input checked="" type="checkbox"/> A full description of the statistical parameters including central tendency (e.g. means) or other basic estimates (e.g. regression coefficient) AND variation (e.g. standard deviation) or associated estimates of uncertainty (e.g. confidence intervals) |
| <input type="checkbox"/> | <input checked="" type="checkbox"/> For null hypothesis testing, the test statistic (e.g. <i>F</i> , <i>t</i> , <i>r</i>) with confidence intervals, effect sizes, degrees of freedom and <i>P</i> value noted
<i>Give P values as exact values whenever suitable.</i> |
| <input type="checkbox"/> | <input checked="" type="checkbox"/> For Bayesian analysis, information on the choice of priors and Markov chain Monte Carlo settings |
| <input type="checkbox"/> | <input checked="" type="checkbox"/> For hierarchical and complex designs, identification of the appropriate level for tests and full reporting of outcomes |
| <input checked="" type="checkbox"/> | <input type="checkbox"/> Estimates of effect sizes (e.g. Cohen's <i>d</i> , Pearson's <i>r</i>), indicating how they were calculated |

Our web collection on [statistics for biologists](#) contains articles on many of the points above.

Software and code

Policy information about [availability of computer code](#)

Data collection	No software was used
Data analysis	<div>Single nucleus RNA-seq data analysis We used the Seek Soul Tools(Version 1.2.1) pipeline to process the cleaned reads and generated the transcript expression matrix. Firstly, the cell barcodes and UMI sequences were extracted based on the defined pattern about the localization of the barcode, linker and UMI within a read. The barcode was corrected with whitelist. The corrected barcode, together with UMI, were put in the header of their corresponding reads. Secondly, the reads were mapped to the reference genomes using STAR (Version 2.5.1b). Then, the reads with barcode and UMI information were assigned to the transcriptome using featureCounts of package Subread (Version 1.6.4). Finally, similar to the raw_feature_bc_matrix results of Cell Ranger, the raw UMI count matrix according to barcodes and transcripts was generated. A cell-calling algorithm was used to filter the raw UMI count matrix and the cell only filtered_feature_bc_matrix was obtained. The code used to process snRNA-seq data can be found at https://http://seek soul.seekgene.com/en/v1.2.1. Integration, clustering, visualization, and differential expression analysis were performed using Seurat. To compare cellular profiles with other species, the expression data matrix of liver from Melopsittacus undulatus, Xenopus laevis, Pelodiscus sinensi, Mus musculus and Homo sapiens were collected and re-analyzed using the same criteria. We first generated homologous genes of Melopsittacus undulatus, Xenopus laevis, Mus musculus and Homo sapiens through Orthofinder (Version 2.5.4). We considered one-to-one orthology from all species. In order to compare and analyze liver cell profiles from all species mentioned, we used canonical correlation analysis (CCA) to integrate their data as anchor datasets with dims = 1:40 to batch correction. Based on the shared structure, all batches of data were finally pooled into a single object for downstream analysis. For clustering, 2000 variable genes were used, and mitochondrial genes were removed from the variable gene set before running PCA and calculating clusters using 20 principal components, and a resolution of 0.6. The non-linear dimensional reduction technique was used to visualize and explore these datasets. We used the Wilcoxon rank sum test to find differential expression. We identified differentially</div>

expressed genes by the following criteria: (1) P-value ≤ 0.05 ; (2) $\log_2(\text{fold change [FC]}) \geq 0.2$; and (3) the percentage of cells where the gene is detected in a specific cluster $> 10\%$. The code used to Integration, clustering, visualization, and differential expression analysis can be found at <https://satijalab.org/seurat>.

Statistical analyses were performed on at least three individual datasets and analyzed using GraphPad Prism software (v.9.5.1). Data are mean \pm SEM from at least three independent experiments, performed in triplicates. The one-way ANOVA were used for comparisons for three or more groups. The two-way ANOVA were used for comparisons with multiple factors. The student's t-test was used for comparisons between two groups. For dose-response experiments, data were normalized and analyzed using nonlinear curve fitting for the log (agonist) versus response (three parameters) curves. ANCOVA was performed in R software (version 4.4.0). The R package mainly included "multcomp" (version 1.4-26). The exact value of n (number of biological or experimental replicates) can be found in the figure legends. Statistical significance was defined as: t-test and ANOVA: ****p < 0.0001 ; ***p < 0.001 ; **p < 0.01 ; *p < 0.05 , ANCOVA: p < 0.001 ; p < 0.01 ; p < 0.05 .

List of all the data analysis software:

software version

ImageJ v1.54g

Graph pad v10.2.0

EnVision Manager 1.14.3049.1193

QuantStudioTM Design & Analysis Software v1.5.2

NIS-Elements BR v5.21

Maga v10.2.6

Image labTM Touch Software v2.4.0.03-DEV MODE

TanonImage v1.00

TSE LabMaster v5.2.4

Zen pro 4.0.30319.42000

For manuscripts utilizing custom algorithms or software that are central to the research but not yet described in published literature, software must be made available to editors and reviewers. We strongly encourage code deposition in a community repository (e.g. GitHub). See the Nature Portfolio [guidelines for submitting code & software](#) for further information.

Data

Policy information about [availability of data](#)

All manuscripts must include a [data availability statement](#). This statement should provide the following information, where applicable:

- Accession codes, unique identifiers, or web links for publicly available datasets
- A description of any restrictions on data availability
- For clinical datasets or third party data, please ensure that the statement adheres to our [policy](#)

The dataset about single-nucleus and bulk RNA-sequencing have been deposited in the NCBI database (accession ID: PRJNA1209237; PRJNA1211354). Publicly available datasets and databases used were the following: single nucleus RNA-seq data of Danio rerio: GSE181987, Xenopus laevis: GSM6214275, GSM6214276, Mus musculus: GSE166504, Homo sapiens: GSE158723 (<https://www.ncbi.nlm.nih.gov/>), and Pelodiscus sinensis: J20080062 (<https://ngdc.cncb.ac.cn/>)

Research involving human participants, their data, or biological material

Policy information about studies with [human participants or human data](#). See also policy information about [sex, gender \(identity/presentation\), and sexual orientation](#) and [race, ethnicity and racism](#).

Reporting on sex and gender

Reporting on race, ethnicity, or other socially relevant groupings

Population characteristics

Recruitment

Ethics oversight

Note that full information on the approval of the study protocol must also be provided in the manuscript.

Field-specific reporting

Please select the one below that is the best fit for your research. If you are not sure, read the appropriate sections before making your selection.

☒ Life sciences ☐ Behavioural & social sciences ☐ Ecological, evolutionary & environmental sciences

For a reference copy of the document with all sections, see [nature.com/documents/nr-reporting-summary-flat.pdf](https://www.nature.com/documents/nr-reporting-summary-flat.pdf)

Life sciences study design

All studies must disclose on these points even when the disclosure is negative.

Sample size	n=3-7 individuals/groups
Data exclusions	no data excluded
Replication	Data are mean \pm SEM from at least three independent experiments, performed in technical triplicate.
Randomization	Since this study involves multiple animal species, to ensure consistency, we first selected animals of the same species, strain, coat color, fur color, body size, and age/gender. These animals were then randomly assigned to each group.
Blinding	We were blinded to group allocation during data collection and analysis

Reporting for specific materials, systems and methods

We require information from authors about some types of materials, experimental systems and methods used in many studies. Here, indicate whether each material, system or method listed is relevant to your study. If you are not sure if a list item applies to your research, read the appropriate section before selecting a response.

Materials & experimental systems

n/a	Involved in the study
<input type="checkbox"/>	<input checked="" type="checkbox"/> Antibodies
<input type="checkbox"/>	<input checked="" type="checkbox"/> Eukaryotic cell lines
<input checked="" type="checkbox"/>	<input type="checkbox"/> Palaeontology and archaeology
<input type="checkbox"/>	<input checked="" type="checkbox"/> Animals and other organisms
<input checked="" type="checkbox"/>	<input type="checkbox"/> Clinical data
<input checked="" type="checkbox"/>	<input type="checkbox"/> Dual use research of concern
<input checked="" type="checkbox"/>	<input type="checkbox"/> Plants

Methods

n/a	Involved in the study
<input checked="" type="checkbox"/>	<input type="checkbox"/> ChIP-seq
<input checked="" type="checkbox"/>	<input type="checkbox"/> Flow cytometry
<input checked="" type="checkbox"/>	<input type="checkbox"/> MRI-based neuroimaging

Antibodies

Antibodies used	<p>GCGR, General gene, UPA61074 beta Actin Ab (HRP), Abways, AB2001 HRP Anti-DDDDK tag, Abcam, ab49763 Goat Anti-Mouse IgG (HRP), Abways, AB0102 Goat Anti-Rabbit IgG (HRP), Abways, AB0101 HRP Anti-DDDDK tag, Sigma, A8592 anti-insulin, Cell Signaling Technnology, 23413S anti-glucagon, Cell Signaling Technnology, 8233S Alexa Fluor 488 conjugated Anti-rabbit, Cell Signaling Technnology, 4412S V5-tag, Cell Signaling Technnology, 13202S</p>
Validation	<p>GCGR constructs from different species with an N-terminal FLAG tag were cloned into pcDNA3.1 (fusion expression) and transiently transfected into HEK293T cells. Western blot (WB) analysis was performed using anti-FLAG and anti-GCGR antibodies to detect protein expression levels, and band size comparison was used to validate the antibody efficacy.</p>

Eukaryotic cell lines

Policy information about [cell lines and Sex and Gender in Research](#)

Cell line source(s)	HEK293 (human fetal kidney), HEK293T (human fetal kidney) cells and AML12 (alpha mouse liver 12) were all obtained from National Collection of Authenticated Cell Cultures (Chinese Academy of Sciences, Shanghai, China). LMH cells (chicken hepatocellular carcinoma epithelial) were obtained from American type culture collection (ATCC, No. CRL-2117)
Authentication	HEK293, HEK293T, AML12, and LMH cells were authenticated by short tandem repeat (STR) testing.
Mycoplasma contamination	Cell lines were tested negatively for mycoplasma by qPCR in the lab

Commonly misidentified lines
(See [ICLAC](#) register)

no commonly misidentified cell lines used in the study

Animals and other research organisms

Policy information about [studies involving animals; ARRIVE guidelines](#) recommended for reporting animal research, and [Sex and Gender in Research](#)

Laboratory animals

Common name	Current scientific name	Age	Gender
Placental mammals			
Rhesus monkey	Macaca mulatta	4years	Male
Mouse(C57BL/6JGpt)	Mus musculus	6-8weeks	Male
Norway rat	Rattus norvegicus	3month	Male
Cattle	Bos taurus	8month	Male
Goat	Capra hircus	8month	Male
Non-placental mammals			
Sugar glider	Petaurus breviceps	4month	Male
Birds			
Common ostrich	Struthio camelus	2years	Male
Chinese yellow-feathered broiler	Gallus gallus	60-90day	Male/Female
Chicks	Gallus gallus	30day	Male
Chicken	Gallus gallus	1 month -3 years	Male
Mallard	Anas platyrhynchos	15-17month	Male
Pigeon	Columba livia	140days	Male
Budgerigar	Melopsittacus undulatus	180days	Male
Vinaceous Rosefinch	Carpodacus vinaceus	1-2years	Male
White-rumped munia	Lonchura striata	3month	Male
Common canary	Serinus canaria	8month	Male
Zebra finch	Taeniopygia guttata	5-6month	Male
Ferruginous flycatcher	Muscicapa ferruginea	8month	Male
Green-backed Tit	Parus monticolus	180days	Male
House sparrow	Passer domesticus	1year	Male
Large-billed leaf warbler	Phylloscopus magnirostris	7month	Male
Red-flanked bluetail	Tarsiger cyanurus	8month	Male
Reptiles			
Green anole	Anolis carolinensis	12-14month	Male
Western painted turtle	Chrysemys picta bellii	4years	Male
Leopard gecko	Eublepharis macularius	1.1years	Male
Peking gecko	Gekko swinhonis	3years	Male
Papenfuss rock agama	Laudakia papenfussi	2years	Male
Kashmir rock agama	Laudakia tuberculata	2years	Male
Theobald's toad-headed agama	Phrynocephalus theobaldi	2years	Male
Chinese blue-tailed skink	Plestiodon chinensis	3years	Male
Anan's rock agama	Laudakia sacra	2years	Male
Central bearded dragon	Pogona vitticeps	1year	Male
Painted turtle	Chrysemys picta picta	3years	Male
Siamese crocodile	Crocodylus siamensis	10years	Male
Beauty rat snake	Elaphe taeniura	18month	Male
Beauty snake	Orthriophis taeniurus	24month	Male
Taiwan stink snake	Elaphe carinata	4years	Male
Mongolia racerunner	Eremias argus	2years	Male
Amphibians			
African clawed frog	Xenopus laevis	1years	Male
Dark-spotted frog	Pelophylax nigromaculatus	2years	Male
Fish			
Zebrafish	Danio rerio	3-5month	Male
Channel catfish	Ictalurus punctatus	2years	Male

Wild animals

No wild animal was used in this study

Reporting on sex

males

Field-collected samples

o field collected samples were used in the study.

Ethics oversight

All animal care and experimental procedures complied with the Animal Management Regulations of the Ministry of Health, China (Document No. 55, 2001) and were approved by the Science and Technology Department of Jiangsu Province [IACUC-20231210].

Note that full information on the approval of the study protocol must also be provided in the manuscript.

Seed stocks	Report on the source of all seed stocks or other plant material used. If applicable, state the seed stock centre and catalogue number. If plant specimens were collected from the field, describe the collection location, date and sampling procedures.
Novel plant genotypes	Describe the methods by which all novel plant genotypes were produced. This includes those generated by transgenic approaches, gene editing, chemical/radiation-based mutagenesis and hybridization. For transgenic lines, describe the transformation method, the number of independent lines analyzed and the generation upon which experiments were performed. For gene-edited lines, describe the editor used, the endogenous sequence targeted for editing, the targeting guide RNA sequence (if applicable) and how the editor was applied.
Authentication	Describe any authentication procedures for each seed stock used or novel genotype generated. Describe any experiments used to assess the effect of a mutation and, where applicable, how potential secondary effects (e.g. second site T-DNA insertions, mosaicism, off-target gene editing) were examined.